

Effective Isentropic Diffusivity of Tropospheric Transport

GANG CHEN

Department of Earth and Atmospheric Sciences, Cornell University, Ithaca, New York

ALAN PLUMB

Program in Atmospheres, Oceans and Climate, Massachusetts Institute of Technology, Cambridge, Massachusetts

(Manuscript received 22 October 2013, in final form 6 May 2014)

ABSTRACT

Tropospheric transport can be described qualitatively by the slow mean diabatic circulation and rapid isentropic mixing, yet a quantitative understanding of the transport circulation is complicated, as nearly half of the isentropic surfaces in the troposphere frequently intersect the ground. A theoretical framework for the effective isentropic diffusivity of tropospheric transport is presented. Compared with previous isentropic analysis of effective diffusivity, a new diagnostic is introduced to quantify the eddy diffusivity of the near-surface isentropic flow. This diagnostic also links the effective eddy diffusivity directly to a diffusive closure of eddy fluxes through a finite-amplitude wave activity equation.

The theory is examined in a dry primitive equation model on the sphere. It is found that the upper troposphere is characterized by a diffusivity minimum at the jet's center with enhanced mixing at the jet's flanks and that the lower troposphere is dominated by stronger mixing throughout the baroclinic zone. This structure of isentropic diffusivity is generally consistent with the diffusivity obtained from the geostrophic component of the flow. Furthermore, the isentropic diffusivity agrees broadly with the tracer equivalent length obtained from either a spectral diffusion scheme or a semi-Lagrangian advection scheme, indicating that the effective diffusivity of tropospheric transport is largely dictated by large-scale stirring rather than details of the small-scale diffusion acting on the tracers.

1. Introduction

The global atmospheric circulation can transport air masses and constituents by either mean advection or eddy diffusion. Using a Green's function diagnostic, Bowman and collaborators (Bowman and Carrie 2002; Bowman and Erukhimova 2004; Erukhimova and Bowman 2006) concluded that tropospheric transport can be described qualitatively by the slow mean diabatic circulation and rapid isentropic mixing. In the observations, the mean diabatic circulation exhibits an equator-to-pole cell, with poleward circulations in the stratosphere and in the upper troposphere and an equatorward return flow near the surface (e.g., Tanaka et al. 2004).

The isentropic mixing in tropospheric transport is not well understood. This is largely due to the complex

boundary condition that nearly half of the isentropes in the troposphere frequently intersect the ground. This near-surface branch of isentropic flow is important for the transport of air pollutants from midlatitude industrialized regions to Arctic upper troposphere. Furthermore, even for the isentropic flow that does not intersect the ground, the recent study by Birner et al. (2013) emphasized the upgradient potential vorticity (PV) fluxes near the subtropical jet, which poses a challenge to the diffusive closure theory of eddy PV fluxes (e.g., Held and Larichev 1996; Lapeyre and Held 2003). The focus of this study is to develop a quantitative framework to assess the effective diffusivity of isentropic mixing in tropospheric transport, especially for the near-surface isentropic flow that frequently intersects the ground.

Much of our understanding of isentropic mixing has been developed by using a quasi-conservative tracer as the meridional coordinate, which separates irreversible mixing from reversible undulation of tracer contours (e.g., Butchart and Remsberg 1986; Nakamura 1995). More specifically, Nakamura (1996) showed that a passive

Corresponding author address: Gang Chen, Dept. of Earth and Atmospheric Sciences, Cornell University, 306 Tower Road, Ithaca, NY 14853.
E-mail: gc352@cornell.edu

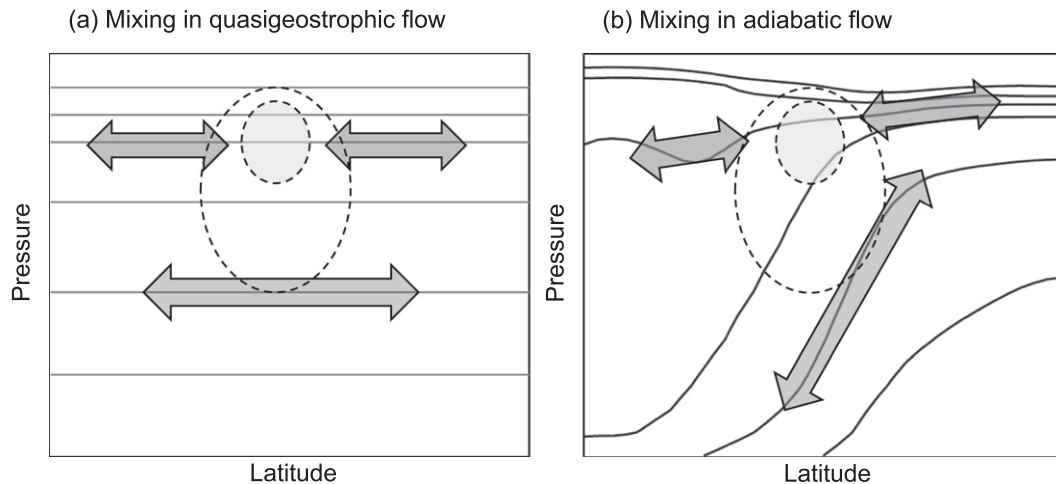


FIG. 1. Schematic diagrams of eddy mixing in (a) quasigeostrophic flow and (b) adiabatic flow. Solid lines denote isobars in (a) and isentropes in (b). Dashed lines and light shading indicate a westerly jet. Arrows denote the directions and strengths of eddy mixing.

tracer advected by a 2D nondivergent flow with pure horizontal diffusion can be formulated in a diffusive form and that the “effective diffusivity” can be defined by the mass flux across the tracer contours. Using a passive tracer driven by the nondivergent isentropic winds in the stratosphere and in the upper troposphere, the effective diffusivity can characterize enhanced mixing within the surf zone and mixing barriers at the subtropics and at the polar vortex edge (Haynes and Shuckburgh 2000a,b; Allen and Nakamura 2001). This diagnostic can be further generalized to the 3D flow, leading to an exact advection–diffusion equation with mass and entropy as the meridional and vertical coordinates, respectively (Nakamura 1998). More recently, Leibensperger and Plumb (2014) extended Nakamura’s formalism of effective diffusivity from pure horizontal diffusion to both isentropic and diabatic diffusions. This extension takes into account the vertical parcel displacement for the small-scale diffusion, which is deemed crucial, since the stirred tracer filaments become thinner and shallower in typical baroclinic flows (Haynes and Anglade 1997). Despite these successes in quantifying isentropic mixing, most studies have assumed that the latitudinal change of isentropic static stability is small, which cannot be applied to the near-surface isentropic flow, where the isentropic air mass converges to zero at the ground.

To circumvent the difficulty in dealing with the near-surface isentropic flow, quasigeostrophic (QG) scaling, in which the isentropic slope is small, is often used. Indeed, studies of the equilibration of baroclinic eddies in the two-layer QG models (e.g., Lee and Held 1993) reveal that the upper troposphere is characterized by wavelike disturbances with enhanced mixing on the jet’s flanks, analogous to the isentropic mixing at the polar

night jet. The lower troposphere, in contrast, is dominated by chaotic mixing throughout the baroclinic zone, and the eddy diffusivity can be parameterized by the mean state (e.g., Held and Larichev 1996; Lapeyre and Held 2003). Using the concept of effective diffusivity, Greenslade and Haynes (2008) quantified the vertical transition from the wavelike upper-level disturbance to lower-level chaotic mixing; they emphasized a sharp vertical transition in effective diffusivity and that the transitional height varies with external parameters such as the beta effect, thermal relaxation rate, and surface friction. Furthermore, Greenslade and Haynes (2008) argued that the vertical transition of diffusivity in a QG model, depicted in Fig. 1a, is analogous to that in a primitive equation model, as illustrated in Fig. 1b. These characteristics are generally consistent with the structure of eddy diffusivity inferred from a gradient–flux relationship of tracer transport (e.g., Plumb and Mahlman 1987) or PV mixing (e.g., Jansen and Ferrari 2013).

Mathematically, the QG diffusivity may be related to the isentropic diffusivity by a local coordinate rotation. For pure isentropic stirring, the diffusivity tensor \mathbf{K} in the y – z plane can be obtained from the isentropic diffusivity K^θ as (e.g., Plumb and Mahlman 1987)

$$\mathbf{K} = \begin{pmatrix} K_{yy} & K_{yz} \\ K_{zy} & K_{zz} \end{pmatrix} = K^\theta \begin{pmatrix} 1 & S_\theta \\ S_\theta & S_\theta^2 \end{pmatrix}, \quad (1)$$

where we have assumed the isentropic slope S_θ is small. Under this small-isentropic-slope assumption, the isentropic diffusivity is equal to the QG diffusivity K_{yy} . This assumption, however, breaks down for the near-surface isentropic flow. It then remains unclear to what extent the QG diffusivity is quantitatively comparable with the

isentropic diffusivity. In this work, we will develop a framework to compare the two diffusivities directly.

Recently, Nakamura and Zhu (2010) showed that under adiabatic conditions, an exact relationship can be obtained between the eddy QG PV flux and the effective diffusion across PV contours, with additional contributions from the change of transient wave activity:

$$\frac{\partial A_{\text{QG}}}{\partial t} + \overline{v'q'_{\text{QG}}} = -\frac{K_{\text{eff}}}{a} \frac{\partial Q_{\text{QG}}}{\partial \phi_e}, \quad (2)$$

where A_{QG} is the QG wave activity, $\overline{v'q'_{\text{QG}}}$ is the eddy QG PV flux, $(1/a)(\partial Q_{\text{QG}}/\partial \phi_e)$ is the Lagrangian meridional gradient of q_{QG} , and K_{eff} is the effective diffusivity. In the time mean, transient wave activities would vanish, resulting in an exact diffusive closure of eddy QG PV fluxes. This seems to be contradictory to the upgradient PV fluxes in the observations (Birner et al. 2013). However, the positive-definite K_{eff} is ensured only for the regular diffusion. As most climate models or chemical transport models use hyperdiffusion or implicit small-scale diffusion that does not guarantee positive-definite values of K_{eff} , it is not clear if Eq. (2) is directly inconsistent with the upgradient PV flux in the observations. In light of this dependence on diffusion scheme, we will introduce a new effective diffusivity definition by the small-scale diffusion experienced by tracers.

We first extend previous formalism of effective diffusivity (Haynes and Shuckburgh 2000a,b; Allen and Nakamura 2001) to deal with the intersections of isentropes with the ground. A new definition of effective diffusivity from the small-scale diffusion experienced by a tracer is introduced to account for both horizontal and vertical parcel displacements. Next, passive tracers are used to diagnose the effective diffusivities induced by the QG flow and adiabatic flow simulated in a dry primitive equation model on the sphere. More specifically, the QG diffusivity is obtained by advecting a tracer with the geostrophic flow at each model level. The adiabatic flow is approximated by eliminating the transformed Eulerian-mean (TEM) residual circulation from the advecting velocities, and therefore the residual tracer transport is expected to be parallel to the isentropic surfaces (e.g., Andrews and McIntyre 1978; Plumb and Ferrari 2005). It is found that while the directions of eddy mixing and the resulting tracer isopleth slopes are different for the QG and adiabatic flows, the patterns of the QG and isentropic effective diffusivities agree quite well. This directly supports the analogy between the QG and isentropic diffusivities. Furthermore, in spite of the upgradient QG PV fluxes near the jet core, the time-mean diffusivities are positive near the jet, implying downgradient eddy tracer fluxes.

The paper is organized as follows. The theory of effective diffusivity is described in section 2. The primitive equation model and idealized numerical experiments are presented in section 3. The diffusivity diagnostics are applied to the tracer transport in the idealized simulations in section 4. Concluding remarks are provided in section 5. Some detailed derivations are provided in the appendix.

2. Theory of effective diffusivity

a. Modified Lagrangian-mean (MLM) diagnostics

Following the isentropic MLM diagnostics reviewed by Nakamura (1998), we first describe a diagnostic framework that allows a direct comparison between the QG and isentropic diffusivities with a change in the vertical coordinate. More specifically, the QG flow can be denoted by the horizontal flow in the pressure coordinate, which can be approximated¹ by the sigma coordinate $\eta = p/p_s$ in a numerical model with a flat lower boundary; the adiabatic flow can be denoted by the horizontal flow in the isentropic coordinate $\eta = \theta$. Using a general vertical coordinate that includes both cases, denoted by η , the governing equation for the tracer q (i.e., either a chemical tracer or a dynamical tracer like PV) advected by a pure horizontal flow in the η coordinates (i.e., $\dot{\eta} = 0$) is

$$\frac{Dq}{Dt} = \frac{\partial q}{\partial t} + \mathbf{v} \cdot \nabla_{\eta} q = \dot{q}, \quad (3)$$

where $\mathbf{v} = (u, v)$ and ∇_{η} are the horizontal velocity and gradient operator at a constant η level and \dot{q} is the sources or sinks of q . We assume that the tracer is conserved except for the small-scale horizontal or vertical diffusion. In the presence of eddy stirring, the effective diffusion is enhanced as a result of the stretching and thinning of tracer material lines.

The mass-density function in η coordinates can be written as

$$\sigma \equiv \frac{1}{g} \left| \frac{\partial p}{\partial \eta} \right| \mathcal{H}(p_s - p). \quad (4)$$

Here $\mathcal{H}(p_s - p)$ is a Heaviside step function for the surface boundary condition (e.g., Nakamura and Solomon 2011). The corresponding continuity equation is

¹We have performed direct calculations with the pressure coordinates for the QG flow. The results in pressure coordinates are very similar to those in sigma coordinates, but the pressure coordinates have to deal with missing values near the surface when the ground does not coincide with an isobaric surface.

$$\frac{\partial \sigma}{\partial t} + \nabla_{\eta} \cdot (\sigma \mathbf{v}) = 0. \quad (5)$$

For the QG flow (i.e., $\sigma = 1/g$), the continuity equation reduces to a nondivergent constraint. For the isentropic flow intersecting the ground, the isentropic mass density transitions to zero below the ground. Therefore, unlike the nondivergent QG flow, the adiabatic flow is convergent near the surface and the formalism of Nakamura (1996) needs to be modified.

We also use the following notations for the Eulerian mass-weighted zonal mean and the deviation therefrom (e.g., Andrews et al. 1987):

$$\overline{X}^* = \overline{\sigma X} / \overline{\sigma} \quad \text{and} \quad \hat{X} = X - \overline{X}^*. \quad (6)$$

Here, the overbars denote zonal means. If the isentropic mass density does not change in time, we see from Eq. (5) that the mean meridional mass flux vanishes ($\overline{v}^* = 0$). For the QG flow, the mass-weighted means reduce to zonal means.

Next, we formulate an MLM tracer equation as in Nakamura (1998). As the isentropic MLM formalism of Nakamura is based on mass continuity, which does not depend on the vertical coordinate used, the MLM formalism of the η coordinates can be obtained by changing the symbols from potential temperature θ and $\dot{\theta}$ to η and $\dot{\eta}$. More specifically, we consider the two-dimensional distribution of the tracer q on a constant η surface. The mass budget enclosed within the tracer contour $q = Q$ can be illustrated in Fig. 2a. We assume that the tracer generally varies monotonically in latitude from the South Pole to the North Pole. The instantaneous spatial distribution of the tracer field may be strongly disturbed by the extreme weather events, with “islands” isolated from the main vortex in the surf zone.

The mass at each η level is often inconvenient to use as a meridional coordinate because of its large variation in the vertical. Instead, the mass encircled by the contour Q toward the North Pole can be used to define a mass equivalent latitude ϕ_e (Nakamura and Solomon 2011) by equalizing the following two mass-weighted area integrals:

$$m(Q, \eta, t) = \iint_{q>Q} \sigma dS = \iint_{\phi>\phi_e} \sigma dS, \quad (7)$$

where $dS = a^2 \cos(\phi) d\lambda d\phi$ is an area element. For the convenience of notation, we have assumed that q has a maximum at the North Pole for the rest of the paper. If q has a minimum at the North Pole, then the inequality in $q > Q$ should be reversed. At a constant η surface, Eq. (7) yields a monotonic relationship from Q to the mass equivalent latitude $\phi_e(Q)$ by

$$\left(\frac{\partial m}{\partial \phi_e} \right)_{\eta} = -2\pi \overline{\sigma} a^2 \cos(\phi_e). \quad (8)$$

Here, the subscript denotes the coordinate held fixed when evaluating the partial derivation. If the zonal mean mass density $\overline{\sigma}$ is independent of latitude, $m/\overline{\sigma}$ reduces to the area and ϕ_e is the familiar area equivalent latitude of Butchart and Remsburg (1986).

Following Nakamura (1995), we can define the Lagrangian area integral by the mass-weighted integral at constant η for the area encircled by the contour $q = Q$ toward the North Pole (shading in Fig. 2a):

$$\mathcal{M}(X) = \iint_{q>Q} \sigma X dS = \int_{q>Q} dq \oint \sigma X \frac{dl}{|\nabla_{\eta} q|}. \quad (9)$$

And the MLM of X can be defined as the mass-weighted average at the Q contour

$$\langle X \rangle = \frac{\partial \mathcal{M}(X) / \partial Q}{\partial m / \partial Q} = \oint_{q=Q} \sigma X \frac{dl}{|\nabla_{\eta} q|} / \oint_{q=Q} \sigma \frac{dl}{|\nabla_{\eta} q|}. \quad (10)$$

By definition, we have the MLM $\langle q \rangle = Q$. Hence, the definition of mass equivalent latitude constructs a hybrid Lagrangian–Eulerian diagnostic. We will use ϕ_e as the meridional coordinate for both the Eulerian mass-weighted mean [$\phi = \phi_e$ in Eq. (6)] and MLM [$Q = Q(\phi_e)$ in Eq. (10)], and it corresponds to the mass poleward of the latitude ϕ_e and the tracer contour $Q(\phi_e)$, respectively.

As in Nakamura (1995), the continuity equation for a pure horizontal flow in the coordinates (Q, η, t) can be written as

$$\left(\frac{\partial m}{\partial t} \right)_{Q, \eta} + \left[\frac{\partial \mathcal{M}(\dot{q})}{\partial Q} \right]_{\eta, t} = 0. \quad (11)$$

In the absence of the small-scale diffusion, this yields no change in the mass bounded by the tracer contour, $(\partial m / \partial t)_{Q, \eta} = 0$. It should be noted that the tracer distribution does not have to be connected in the physical space. For example, the blob detached from the main vortex in Fig. 2a can merge again with the main vortex. If no dissipation takes place, the blob remains as a part of the main vortex in the Q -based coordinate throughout the reversible detachment and merging.

Furthermore, the rate of change for the mass poleward of ϕ_e can be obtained from Eqs. (5) and (7):

$$\left(\frac{\partial m}{\partial t} \right)_{\phi_e, \eta} = \frac{\partial}{\partial t} \iint_{\phi>\phi_e} \sigma dS = 2\pi a \cos(\phi_e) \overline{\sigma} \overline{v}^*. \quad (12)$$

Unlike the mass bounded by the tracer contour, the mass poleward of a latitude can change because of

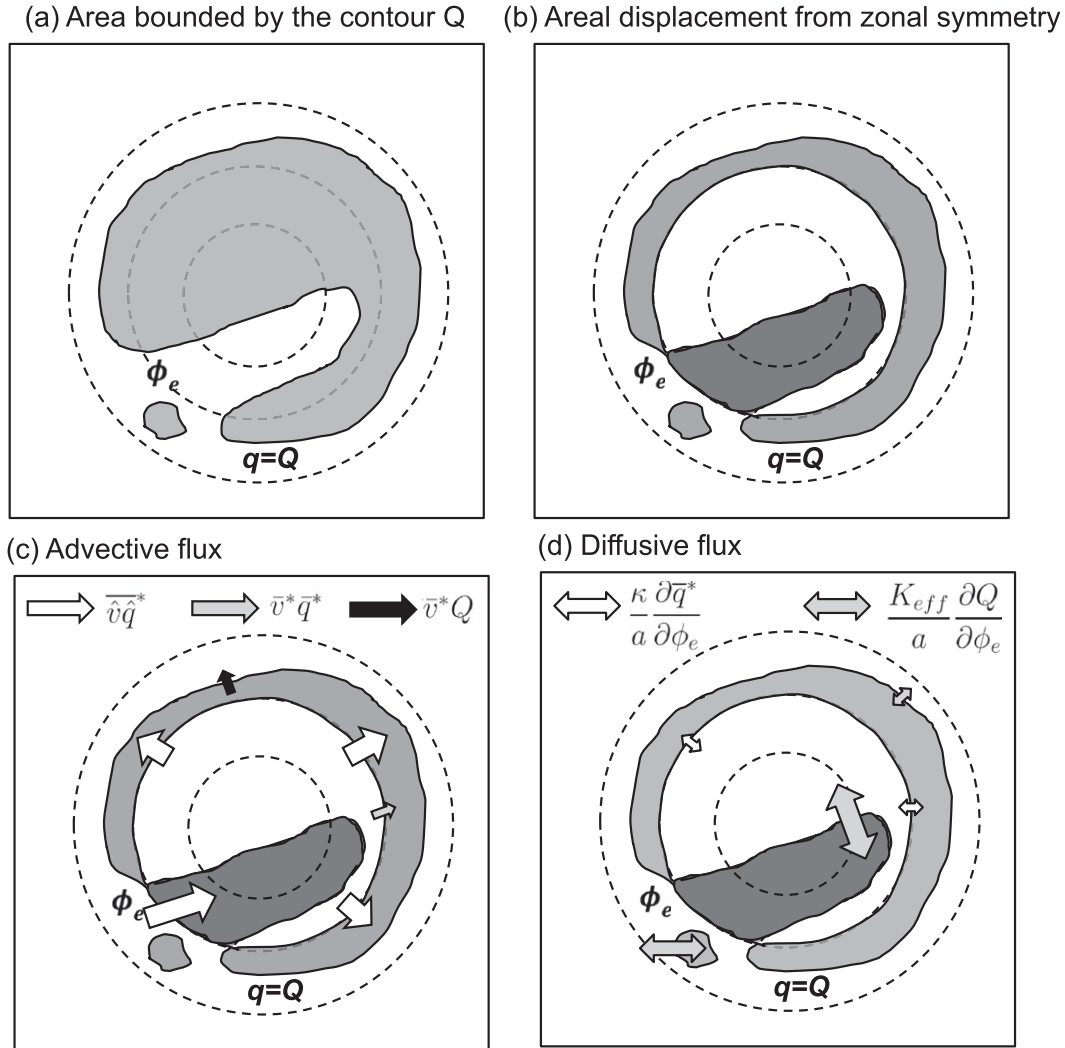


FIG. 2. Schematics of a quasi-conservative tracer q associated with an idealized wave-breaking event in the polar stereographic projection. The tracer is advected by pure horizontal motions on a constant η surface (i.e., $\eta = 0$). Dashed concentric circles denote the latitude circles. (a) Shading highlights the area between the tracer contour $q = Q$ and the pole, and the mass bounded by Q is the same as the mass between latitude ϕ_e and the pole. (b) Shading denotes the areal displacement from zonal symmetry, where light shading denotes the equatorward flow across latitude ϕ_e and dark shading denotes the poleward flow. (c) The advective contributions to the wave activity variability in Eq. (29) is represented by arrows: the eddy advective flux (white), the mean advection across the latitude ϕ_e (gray), and the mean advection across the contour Q (black). The net mean advection is equal to the advection of wave activity $(\bar{v}^*/a)\partial[A \cos(\phi_e)]/\partial\phi_e = \bar{\sigma}\bar{v}^* \cos(\phi_e)(\bar{q}^* - Q)$. (d) The diffusive contributions to the wave activity variability are represented by arrows: diffusive flux across latitude ϕ_e (white) and the flux across the contour Q (gray). Their difference gives the eddy diffusive flux $(K_{eff}^e/a)\partial Q/\partial\phi_e = (K_{eff}/a)\partial Q/\partial\phi_e - (\kappa/a)\partial\bar{q}^*/\partial\phi_e$. See the text in section 2 for details.

instantaneous meridional mass flux across the latitude even for a conservative (i.e., frictionless and adiabatic) flow. More precisely, we can make the meridional coordinate transformation from Q to ϕ_e :

$$\left(\frac{\partial m}{\partial t}\right)_{Q,\eta} = \left(\frac{\partial m}{\partial t}\right)_{\phi_e,\eta} - \left(\frac{\partial m}{\partial Q}\right)_{\eta,t} \left(\frac{\partial Q}{\partial t}\right)_{\phi_e,\eta}. \quad (13)$$

Finally, substituting Eqs. (13) and (12) into Eq. (11) and dividing by $-(\partial m/\partial Q)_{\eta,t}$ gives an MLM tracer

equation, which can be also obtained from Eq. (36) in Nakamura (1998) by using $\dot{\theta} = 0$:

$$\frac{\partial Q}{\partial t} + \frac{\bar{v}^*}{a} \frac{\partial Q}{\partial \phi_e} = \langle \dot{q} \rangle, \quad (14)$$

where we have used Eq. (7) to replace m with ϕ_e . For pure horizontal motions, we see that in addition to the small-scale diffusion, the MLM at ϕ_e can be affected by \bar{v}^* . This formula holds exactly for the

convergent isentropic flow that intersects the ground. In the case of the QG flow, Eq. (14) reduces to a pure diffusive form as in Nakamura (1996).

b. Definition of effective diffusivity with tracer gradients

Using a single-layer model, the effective diffusivity can be obtained directly by solving the tracer equation [Eq. (3)] using the meteorological winds with explicit diffusion (e.g., Haynes and Shuckburgh 2000a,b; Allen and Nakamura 2001). Consider a tracer advected by pure horizontal flow (i.e., $\dot{\eta} = 0$) and subject to the horizontal diffusion

$$\dot{q} = \frac{1}{\sigma} \nabla_{\eta} \cdot (\sigma \kappa \nabla_{\eta} q), \quad (15)$$

where κ is the diffusion coefficient and σ is included for the surface boundary condition. The MLM tracer equation [Eq. (14)] can be written as

$$\frac{\partial Q}{\partial t} + \frac{\bar{v}^*}{a} \frac{\partial Q}{\partial \phi_e} = \frac{1}{a^2 \bar{\sigma} \cos(\phi_e)} \frac{\partial}{\partial \phi_e} \left[\bar{\sigma} \cos(\phi_e) K_{\text{eff}} \frac{\partial Q}{\partial \phi_e} \right], \quad (16)$$

where the effective diffusivity is defined as

$$K_{\text{eff}} = a^2 \left(\frac{\partial Q}{\partial \phi_e} \right)^{-2} \langle \kappa |\nabla_{\eta} q|^2 \rangle. \quad (17)$$

The derivations of the effective diffusivity follow Nakamura (1996) with the additional mass density σ for surface boundary condition. By construction, K_{eff} is positive definite. If $\bar{\sigma}$ is independent of latitude, Eqs. (16) and (17) reduce to their nondivergent analogs (Nakamura 1996; Shuckburgh and Haynes 2003). As such, in spite of different mixing directions, the QG and isentropic effective diffusivities can be compared in a single diagnostic framework.

If the form of the small-scale diffusion is unknown, we can define a nondimensional measure of eddy mixing by tracer contours as (Haynes and Shuckburgh 2000a; Allen and Nakamura 2001):

$$\tilde{K}_{\text{eff}} = a^2 \left(\frac{\partial Q}{\partial \phi_e} \right)^{-2} \langle |\nabla_{\eta} q|^2 \rangle = \frac{L_{\text{eq}}^2}{[2\pi a \cos(\phi_e)]^2}, \quad (18)$$

where L_{eq} is the equivalent length of a tracer contour and $L_{\text{eq}} \geq L$ [L is the actual length of the tracer contour; see Haynes and Shuckburgh (2000a)]. Here, $2\pi a \cos(\phi_e)$ is the minimum length of a tracer contour. If the tracer contour is zonally symmetric, this yields the minimum value $\tilde{K}_{\text{eff}} = 1$.

c. Definition of effective eddy diffusivity with small-scale diffusion

When the isentropic layer intersects the ground, it becomes complex to compute the small-scale diffusion in a single-layer model. To avoid this complexity, we consider a 3D model, in which the small-scale diffusion can be applied along the model layer at the ground rather than along the isentropic layer. Therefore, the small-scale diffusion would include both horizontal parcel displacements along isentropes and vertical displacements across the isentropes, and an effective diffusivity definition like Eq. (17) is discussed in Leibensperger and Plumb (2014). While the effective diffusivity of Nakamura (1996) considers the diffusive flux across tracer contours, we introduce a new definition by integrating the small-scale diffusion over the vicinity of finite-amplitude waves. More specifically, the effective diffusivity is defined by the small-scale diffusion diagnosed in the model as

$$K_{\text{eff}}^e = -\frac{a}{\bar{\sigma}} \left(\frac{\partial Q}{\partial \phi_e} \right)^{-1} \Delta \mathcal{M}(\dot{q}), \quad (19)$$

where the superscript e indicates eddy diffusivity, and the eddy operator $\Delta(X)$ is defined as

$$\begin{aligned} \Delta \mathcal{M}(X) &= \frac{1}{2\pi a \cos(\phi_e)} \left[\iint_{q>Q} \sigma X \, dS - \iint_{\phi>\phi_e(Q)} \sigma X \, dS \right] \\ &= \frac{1}{2\pi a \cos(\phi_e)} \left[\iint_{q>Q, \phi \leq \phi_e(Q)} \sigma X \, dS - \iint_{\phi>\phi_e(Q), q \leq Q} \sigma X \, dS \right]. \end{aligned} \quad (20)$$

Here, $\Delta \mathcal{M}(X)$ in the first line is the difference between the mass-weighted integral from Q toward the pole and the integral poleward of the corresponding $\phi_e(Q)$. The second line also corresponds to the areal displacement

from zonal symmetry shown in Fig. 2b, where the light shading denotes the equatorward flow across ϕ_e and dark shading denotes the poleward flow. Therefore, $\Delta \mathcal{M}(\dot{q})$ denotes the integral of the small-scale diffusion

over the areal displacement of finite-amplitude waves. As the mass poleward of Q is equal to the mass poleward of $\phi_e(Q)$, we have $\Delta\mathcal{M}(1) = 0$ by construction. If the tracer contour is zonally symmetric, $\Delta\mathcal{M}(X) = 0$.

Using this definition of effective diffusivity [Eq. (19)], the MLM tracer equation corresponding to Eq. (14) becomes

$$\frac{\partial Q}{\partial t} + \frac{\bar{v}^*}{a} \frac{\partial Q}{\partial \phi_e} = \frac{1}{a^2 \bar{\sigma} \cos(\phi_e)} \frac{\partial}{\partial \phi_e} \times \left[\bar{\sigma} \cos(\phi_e) K_{\text{eff}}^e \frac{\partial Q}{\partial \phi_e} \right] + \bar{q}^*. \quad (21)$$

Note that the mass density transitions to zero below the ground, which implicitly deals with the ground intersections. If the tracer is subject to the horizontal diffusion as Eq. (15), Eqs. (16) and (17) yield

$$K_{\text{eff}}^e = K_{\text{eff}} - \kappa \frac{\partial \bar{q}^* / \partial \phi_e}{\partial Q / \partial \phi_e}. \quad (22)$$

This suggests that K_{eff}^e is an effective eddy diffusivity that represents the amplification from the small-scale diffusivity κ to K_{eff} of Nakamura (1996) because of eddy stirring.

This effective eddy diffusivity is explained schematically in Fig. 2d. The gray arrows depict the diffusive mass flux across the tracer contour, $(K_{\text{eff}}/a)(\partial Q/\partial \phi_e)$, and the white arrows depict the zonal mean diffusive flux across the latitude, $(\kappa/a)(\partial \bar{q}^*/\partial \phi_e)$. It follows from Eq. (22) that K_{eff}^e is defined by the net diffusive mass flux through the area bounded by Q and ϕ_e . As the diffusive flux across tracer contours is large in the regions of wave breaking and the zonal mean diffusive flux is small, K_{eff}^e represents the enhanced diffusivity as a result of the deviation of tracer contours from zonal symmetry.

Similar to Eq. (18), if the form of the small-scale diffusion is unknown, we can define a measure of eddy mixing with tracer contours as

$$\begin{aligned} \tilde{K}_{\text{eff}}^e &= -\frac{a}{\bar{\sigma}} \left(\frac{\partial Q}{\partial \phi_e} \right)^{-1} \Delta\mathcal{M} \left[\frac{1}{\sigma} \nabla_\eta \cdot (\sigma \nabla_\eta q) \right] \\ &= \frac{L_{\text{eq}}^2}{[2\pi a \cos(\phi_e)]^2} - \frac{\partial \bar{q}^* / \partial \phi_e}{\partial Q / \partial \phi_e}. \end{aligned} \quad (23)$$

Again if the tracer contour is zonally symmetric, $\tilde{K}_{\text{eff}}^e = 0$. Therefore, \tilde{K}_{eff}^e can be thought of as the increase in tracer equivalent length due to eddy stirring and it can be referred to as the eddy equivalent length ratio.

For adiabatic flow, Nakamura (1998) also defined effective diffusivity using the small-scale diffusion experienced by a tracer. However, our definition separates the

diffusivity acting on the mean flow from the diffusivity on the eddy, which is important for a tracer dominated by the small-scale vertical diffusion. That is, the effective isentropic diffusivity should be separate from the effective diabatic diffusivity. More importantly for the small-scale vertical (diabatic) diffusivity, we have assumed that (i) the antidiagonal terms in the effective diffusivity tensor, as formulated in Lebensperger and Plumb (2014), can be ignored, and (ii) the effective diabatic diffusivity is not augmented from the small-scale diabatic diffusivity even in the presence of stirring [formulated as \bar{q}^* in Eq. (21)]. These assumptions are directly supported by an analysis of tracer transport in an idealized stratospheric flow (Lebensperger and Plumb 2014).

Insights into the effective eddy diffusivity can be gained by considering the small-amplitude limit that the meridional displacement of tracer contours is small. The effective diffusivity defined with $\Delta\mathcal{M}(\dot{q})$ can be approximated as (see the appendix)

$$K_{\text{eff}}^e \approx -a^2 \left(\frac{\partial Q}{\partial \phi_e} \right)^{-2} \overline{\hat{q} \hat{q}^*}, \quad (24)$$

where \bar{X}^* and \hat{X} denotes the mass-weighted zonal means of X and deviations therefrom, respectively [Eq. (6)]. Furthermore, the small-scale diffusion acting on the tracer can be written as

$$\dot{q} = \frac{1}{\sigma} \nabla_\eta \cdot (\sigma \kappa_h \nabla_\eta q) + \frac{1}{\sigma} \frac{\partial}{\partial \eta} \left[\sigma \kappa_v \left(\frac{\partial \eta}{\partial z} \right)^2 \frac{\partial q}{\partial \eta} \right], \quad (25)$$

where κ_h is the horizontal diffusion coefficient and κ_v is the vertical (diabatic) diffusion coefficient expressed in the height coordinates. In the small-amplitude limit and assuming that the variance of \hat{q} is almost homogeneous in space, the effective eddy diffusivity (see the appendix) can be approximated as

$$K_{\text{eff}}^e \approx a^2 \left(\frac{\partial Q}{\partial \phi_e} \right)^{-2} \left[\overline{\kappa_h |\nabla_\eta \hat{q}|^2}^* + \kappa_v \left(\frac{\partial \eta}{\partial z} \right)^2 \overline{\left(\frac{\partial \hat{q}}{\partial \eta} \right)^2}^* \right]. \quad (26)$$

This can be thought of as the small-amplitude approximation of the effective diffusivities for the horizontal diffusion in Eq. (17) or for the vertical diffusion examined in Lebensperger and Plumb (2014). In this limit, the effective diffusivity appears to be nonnegative. However, since the variance of \hat{q} is generally spatially inhomogeneous and the eddy amplitude is large in typical baroclinic flow, there is no constraint on the sign of K_{eff}^e . This is also true for hyperviscosity or implicit diffusion that is commonly used in climate models or chemical transport

models. Empirically, we find the time-mean effective diffusivity is positive almost everywhere. If the effective eddy diffusivity dominates over the mean diffusivity \bar{q}^* or mean advection \bar{v}^* , the tracer field is expected to be gradually homogenized along the primary direction of mixing.

d. Eddy diffusive closure

An Eulerian diffusive closure of eddy fluxes can be obtained by examining the tracer variance budget (e.g., Tung 1986; Jansen and Ferrari 2013), and a similar relationship can be derived by means of the tracer mass equivalent latitude. From Eq. (3), the zonal mean tracer tendency at ϕ_e is related to the mean tracer advection, eddy tracer flux, and tracer sources–sinks as [e.g., see appendix of Jansen and Ferrari (2013)]

$$\frac{\partial \bar{q}^*}{\partial t} + \frac{\bar{v}^*}{a} \frac{\partial \bar{q}^*}{\partial \phi_e} = -\frac{1}{a\bar{\sigma} \cos(\phi_e)} \frac{\partial}{\partial \phi_e} [\cos(\phi_e) \bar{\sigma} \bar{v} \bar{q}^*] + \bar{q}^*. \quad (27)$$

Using the finite-amplitude wave activity $A \equiv \Delta \mathcal{M}(q)$ of Nakamura and Solomon (2011) and taking a derivative with respect to the mass $m(Q, \eta, t)$ for Eq. (20), we obtain a relationship between the Eulerian and MLM quantities analogous to the QG PV case (Nakamura and Zhu 2010):

$$Q = \bar{q}^* - \frac{1}{a\bar{\sigma} \cos(\phi_e)} \frac{\partial}{\partial \phi_e} [\cos(\phi_e) A]. \quad (28)$$

This can be used to define the mean advection of wave activity, shown schematically in Fig. 2c. The mean advection across ϕ_e , in the flux form of $\bar{v}^* \bar{q}^*$, is depicted by the gray arrow, and the mean advection across Q , in the flux form of $\bar{v}^* Q$, is depicted by the black arrow. Their net effect yields an advective form of wave activity as $(\bar{v}^*/a) \partial [A \cos(\phi_e)] / \partial \phi_e$. Similarly, the eddy advective flux across ϕ_e , $\bar{v} \bar{q}^*$, is depicted by the white arrows.

It then follows that subtracting Eq. (27) by Eq. (21) yields

$$\frac{\partial [A \cos(\phi_e)]}{\partial t} + \frac{\bar{v}^*}{a} \frac{\partial [A \cos(\phi_e)]}{\partial \phi_e} + \cos(\phi_e) \bar{\sigma} \bar{v} \bar{q}^* = -\frac{\bar{\sigma} \cos(\phi_e) K_{\text{eff}}^e}{a} \frac{\partial Q}{\partial \phi_e}. \quad (29)$$

Particularly, this wave activity budget is built on a hybrid Lagrangian–Eulerian mass budget between Q and ϕ_e as illustrated in Figs. 2c and 2d. The tracer wave activity, defined by the areal displacement of tracer contours from zonal symmetry, is controlled by the net mean advection, eddy advective flux, and diffusive flux through the area bounded by the tracer contour and the latitude.

Hereby we have extended the QG formalism [Eq. (2)] to the effective eddy diffusivity with pure horizontal motions in a general vertical coordinate η . If q denotes the Ertel PV, this also completes the isentropic form of the nonacceleration theorem in Nakamura and Solomon (2011) by the concept of effective diffusivity. Compared with the Eulerian form (e.g., Jansen and Ferrari 2013), the advective flux in the mass equivalent latitude is expressed in a more straight-forward form with the mean meridional mass flux. In the time average, we see that the isentropic eddy flux is maintained by the diffusive flux along the Lagrangian gradient plus an additional advective flux of wave activity. By corollary, the eddy flux is downgradient provided that the advective flux of wave activity is small.

3. Dry primitive equation model

The effective eddy diffusivity defined in Eq. (19) is examined in the simulations of a dry primitive equation model with idealized forcing and dissipation. While moisture is likely to play an important role in the global-scale tropospheric transport (e.g., Erukhimova and Bowman 2006; Hess 2005), a dry primitive equation model is particularly useful to compare the isentropic mixing near the ground with the QG diffusivity (e.g., Lee and Held 1993; Greenslade and Haynes 2008). Here we use the Geophysical Fluid Dynamical Laboratory (GFDL) spectral atmospheric dynamical core with the Held and Suarez (1994) forcing. The model is forced by the Newtonian relaxation to zonally symmetric equilibrium temperature and damped by the Rayleigh friction in the planetary boundary layer. The subgrid diffusion is parameterized by the ∇^8 hyperdiffusion on temperature, vorticity, and divergence, with the damping time scale of 0.1 day at the smallest resolved scale. The results for the ∇^4 hyperdiffusion and varying diffusion coefficients are quantitatively similar and are not reported here. Compared with the Held and Suarez (1994) setup, we introduce an extra parameter ϵ for the hemispheric asymmetry in the radiative equilibrium temperature:

$$T_{\text{eq}} = \max \left\{ 200, \left[315 - \epsilon \sin \phi - 60 \sin^2 \phi - 10 \log \left(\frac{p}{10^5} \right) \cos^2 \phi \right] \left(\frac{p}{10^5} \right)^\kappa \right\}. \quad (30)$$

The parameter is set as $\epsilon = 20$ K (except for the results presented in Figs. 10 and 11), which produces a strong Hadley circulation and an intense subtropical jet in the winter hemisphere.

The model is run at the horizontal resolution T42 and 20 equally spaced sigma vertical levels, and the results

TABLE 1. Descriptions of idealized experiments of tracer transport. See section 3 for details.

Expt	Initial tracer	Numerical scheme	Advecting flow	ϵ in T_{eq} (K)
1	$\sin\phi$	Spectral	Total flow	20
2	$\sin\phi$	Spectral	TEM circulation	20
3a	$\sin\phi$	Spectral	Geostrophic flow	20
3b	$\sin^3\phi$	Spectral	Geostrophic flow	20
3c	$\tanh(2\phi)$	Spectral	Geostrophic flow	20
4a	$\sin\phi$	Spectral	Adiabatic flow	20
4b	$\sin^3\phi$	Spectral	Adiabatic flow	20
4c	$\tanh(2\phi)$	Spectral	Adiabatic flow	20
5a	$\sin\phi$	Spectral	Geostrophic flow	0
5b	$\sin\phi$	Spectral	Geostrophic flow	10
5c	$\sin\phi$	Spectral	Geostrophic flow	30
5d	$\sin\phi$	Spectral	Geostrophic flow	40
6a	$\sin\phi$	Spectral	Adiabatic flow	0
6b	$\sin\phi$	Spectral	Adiabatic flow	10
6c	$\sin\phi$	Spectral	Adiabatic flow	30
6d	$\sin\phi$	Spectral	Adiabatic flow	40
7	$\sin\phi$	Grid	Adiabatic flow	20

are presented in the figures with the sigma level multiplied by 1000 hPa as the vertical coordinate. The model is integrated for 2000 days to reach a statistical equilibrium of baroclinic waves and the next 300 days of the simulation is used to advect passive tracers for diffusivity diagnoses. Passive spectral tracers, advected by the velocities created by the model, are diffused by the same ∇^8 hyperdiffusion as the dynamical fields such as PV or potential temperature. This helps to determine whether the upgradient eddy PV fluxes, if simulated in the model, are associated with negative effective diffusivity or not, since the effective diffusivity of the regular diffusion is positive definite by design. Furthermore, the evolution of the spectral tracer is checked with the grid tracer advected by the same flow with a semi-Lagrangian scheme for horizontal advection (Lin et al. 1994) and a finite-volume parabolic scheme for vertical advection. Since the small-scale diffusion experienced by the grid tracer is implicit, we can only calculate the equivalent length of the tracer contours. Therefore, most of our results are shown for the spectral tracer subject to the hyperdiffusion (except for the grid tracer results in Figs. 12 and 13). A summary of the idealized experiments of tracer transport is documented in Table 1 and described in detail as follows.

Four types of advecting velocities are investigated: the total flow simulated in the model (experiment 1 in Table 1), the TEM residual circulation (experiment 2), the geostrophic flow (experiment 3a), and the adiabatic flow (experiment 4a). The TEM circulation is calculated at each time step in the model sigma coordinate $\eta = p/p_s$ as

$$\bar{v}^r = \frac{1}{\bar{p}_s} \left\{ \bar{p}_s \bar{v} - \frac{\partial}{\partial \eta} \left[\overline{(p_s v)' \theta'} \right] \right\}$$

$$\bar{\eta}^r = \frac{1}{\bar{p}_s} \left\{ \bar{p}_s \bar{\eta} + \frac{1}{a \cos \phi} \frac{\partial}{\partial \phi} \left[\cos \phi \overline{(p_s v)' \theta'} \right] \right\}. \quad (31)$$

where overbars denote the zonal means on a sigma level and primes denote the deviations therefrom. We have used the QG TEM circulation, which is found to be sufficient for our idealized simulations. For more realistic simulations in which the near-surface static stability is neutral, one may use the coordinate-independent TEM circulation (Andrews and McIntyre 1978) or the mean overturning circulation with the mass above isentropes as the vertical coordinates (Chen 2013); both can be formulated on the model sigma levels.

Next, the geostrophic flow is obtained by taking the nondivergent component of the pressure-weighted horizontal velocity (i.e., $p_s \mathbf{v} / \bar{p}_s$) at each sigma level. Furthermore, the adiabatic flow is approximated by subtracting the TEM circulation from the total velocity. This eliminates the diabatic mass fluxes across the isentropic surfaces, and the residual tracer transport is expected to be along isentropic surfaces (e.g., Andrews and McIntyre 1978; Plumb and Ferrari 2005). Consequently, the small-scale diffusion averaged at the tracer contour at an isentropic surface can be written in a diffusive form [i.e., Eq. (21) and $\bar{v}^{*r} \approx 0$ after removing the TEM circulation]. This separation in advecting velocities allows us to understand the effects of different components of the flow on the tracer distribution.

The effective diffusivities are calculated from the tracers advected by the QG flow and adiabatic flow, and additional sensitivity experiments are performed with respect to initial tracer distributions and advecting flows as in Haynes and Shuckburgh (2000a). Three initial distributions [i.e., $\sin(\phi)$, $\sin^3(\phi)$, and $\tanh(2\phi)$] are compared in experiments 3a–3c and experiments 4a–4c. As discussed in Haynes and Shuckburgh (2000a), the initial tracer distribution will adjust to align with the dominant quasi-zonal flow quickly, and the effective diffusivity thereafter is expected to be independent of initial conditions. Furthermore, the strengths of the jets are altered by changing the parameter of hemispherically asymmetric heating from $\epsilon = 0$ to $\epsilon = 40$ K with an interval of 10 K (experiments 5a–5d and 6a–6d). As ϵ gets larger, the jet will be stronger in the winter hemisphere and weaker in the summer hemisphere.

Following Eq. (19), the effective eddy diffusivity is diagnosed with the small-scale diffusion experienced by the

spectral tracers. The area integral with respect to tracer contours is performed with a box counting method as Nakamura and Solomon (2011). For the geostrophic flow, the surface pressure is used as the mass density in the sigma coordinates. As the diffusion is applied along the sigma surface, the diffusivity is also confirmed with the diffusivity definition in Eq. (17) using the tracer gradients. Next, for the isentropic diffusivity, all the variables are first interpolated onto 71 isentropic levels ranging from 240 to 380 K with an increment of 2 K. The mass equivalent latitude facilitates a simple treatment of the surface boundary condition for the isentropic surfaces intersecting the ground (Nakamura and Solomon 2011). The effective diffusivity is diagnosed with the interpolated small-scale diffusion, which includes both isentropic and diabatic diffusions. Finally, as the small-scale diffusion for the grid tracer is implicit, the equivalent length is calculated with the tracer contours using Eq. (23).

4. Tracer transport diagnosis

a. Zonal mean tracer isopleths

We first examine the effects of advecting flows on the zonal mean tracer isopleths. Figure 3 shows the climatological-mean zonal wind, potential temperature, TEM residual circulation, and QG PV flux for the experiments with $\epsilon = 20$ K in the radiative equilibrium temperature. In this configuration, the westerly jet is stronger and slightly more equatorward in the NH (~ 43 m s⁻¹ and 43°N) than in the SH (~ 24 m s⁻¹ and 46°S). The 300- or 310-K isentropic surface extends approximately from the subtropics at the surface to the high latitudes near the tropopause. The TEM residual circulation rises near 15°S in the summer hemisphere. The northern branch of the residual circulation crosses the equator into the winter hemisphere, descends slightly in the subtropics, and finally moves down to the surface in the high latitudes. The summer cell is similar in structure to the winter cell, but the strength is about half of its winter cell. Furthermore, the QG PV fluxes are predominately positive in the lower troposphere and negative in the upper troposphere, as expected from eddy mixing of the background PV gradient. Interestingly, there are noticeable upgradient PV fluxes near the jet core of the winter hemisphere, as found in Birner et al. (2013). All in all, the idealized simulation captures the basic structures of the observed mean circulations in the solstitial season (cf. Haynes and Shuckburgh 2000b; Tanaka et al. 2004; Chen 2013; Birner et al. 2013), while in the observations the wintertime subtropical jet is more equatorward and the subtropical descent of the residual circulation is more distinct from the midlatitude maximum.

The total velocities are used to advect a passive spectral tracer initialized with a $\sin\phi$ distribution, and the zonal mean isopleths on selected days are shown in the left panels of Fig. 4. From days 3 to 30, we see that the initial vertically aligned isopleths (dashed and solid lines) in the extratropics are tilted toward local isentropic surfaces (dashed-dotted lines), and the isopleths in the tropics move upward at 20°S–0° because of the tropical rising branch of the residual circulation (Fig. 3). This results in a local minimum of tracer mixing ratio near 10°N in the lower troposphere. The tracer isopleth slopes remain roughly unchanged from days 30 to 90, although the meridional gradient of tracer mixing ratio on day 90 is much reduced from that on day 30. This suggests that the tracer isopleth slopes may be explained by a balance between the mean advection and eddy mixing as the long-lived tracers in the stratosphere (e.g., Holton 1986; Mahlman et al. 1986). The time scales are consistent with Haynes and Shuckburgh (2000a), who found that the effective diffusivity of the stratosphere is independent of the initial conditions of tracers after a 1-month spinup, and that the effective diffusivity of lower-stratospheric eddy mixing allows the tracer gradients to survive a seasonal cycle. Note that there is no small-scale convection and associated vertical diffusion in this model, and their effects are beyond the scope of this study.

The separate effects of mean advection and mixing are illustrated by advecting the tracer with different components of the flow. When the tracer is advected by the TEM residual circulation shown in the right panels of Fig. 4, the zonal mean tracer isopleths from days 3 to 30 are similar to those advected by the total flow. However, the tracer isopleths on day 90 advected by the TEM circulation differ considerably from those advected by the total flow. If the advecting circulation is steady with no diffusion, the tracer mixing ratio would be homogenized along the streamlines in the steady state, and the equilibrium tracer isopleths would resemble the streamlines. Although the TEM circulation is not exactly steady, the tracer isopleths on day 90 approximately follow the streamlines of the time averaged TEM circulation (cf. Figs. 4 and 3). Interestingly, while the initial tracer mixing ratio is positive everywhere in the NH, negative mixing ratios are found in the NH midlatitudes on day 90, which can be traced back to the upper-level air masses crossing the equator on day 30. It should be noted that the same ∇^8 numerical diffusion is applied to this experiment, but little effective diffusion occurs since the tracer distribution remains zonally symmetric in the absence of eddy stirring. In comparison with the transport by the total flow, we see that the mean mass circulation is important for the tropical ascent and interhemispheric exchange of tracers,

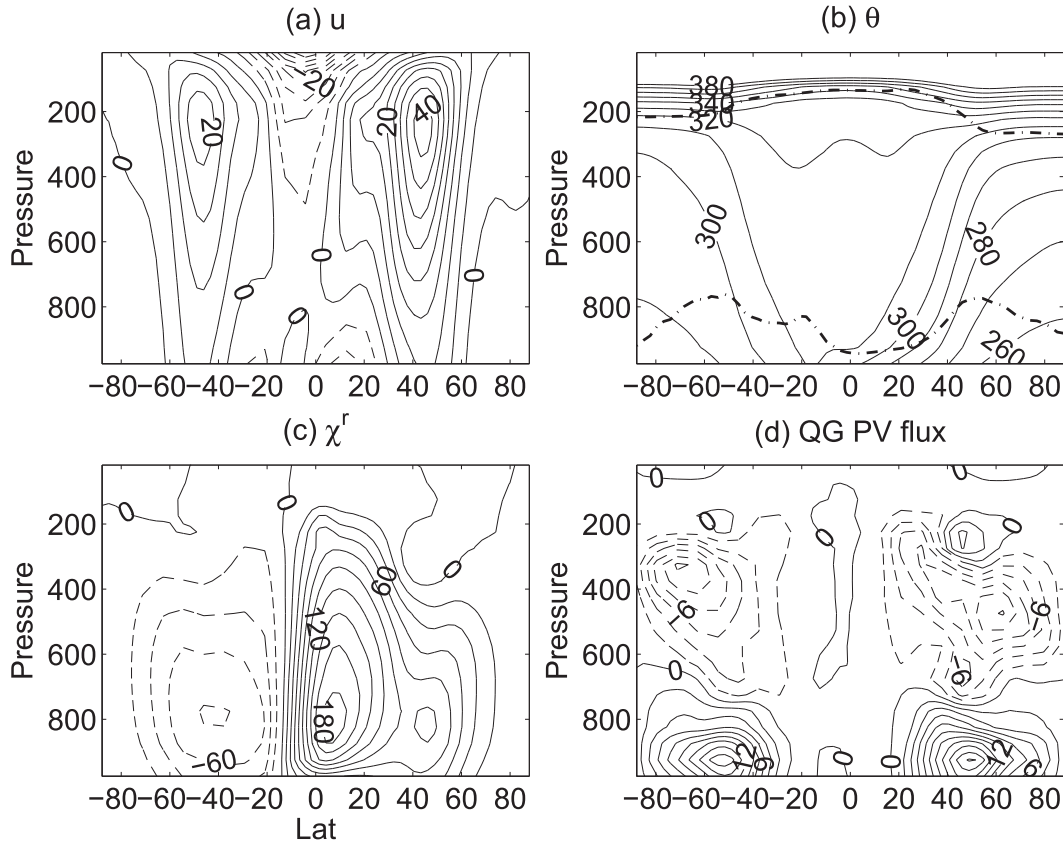


FIG. 3. The climatological-mean (a) zonal wind, (b) potential temperature, (c) TEM residual circulation, and (d) quasigeostrophic potential vorticity flux. The contour intervals are 5 m s^{-1} , 10 K , $20 \times 10^9 \text{ kg s}^{-1}$, and $2 \text{ m s}^{-1} \text{ day}^{-1}$, respectively. The parameter for radiative equilibrium temperature is $\epsilon = 20 \text{ K}$. The dashed-dotted lines in (b) indicate the tropopause defined by the WMO lapse-rate definition and the 95% quantile of the surface temperature distribution. Pressure is the vertical coordinate and hereafter corresponds to the sigma level (p/p_s) multiplied by 1000 hPa.

but the extratropical tracer isopleths depend critically on the eddy mixing.

Turning our attention to eddy mixing, the evolution of the zonal mean tracer isopleths are shown in Fig. 5 for the QG flow in the left panels and for the adiabatic flow in the right panels. In both experiments, the tracer isopleth slopes remain approximately unchanged after day 30. For the QG flow, the primary direction of parcel displacements takes place along the model sigma levels, and for the adiabatic flow, the parcel displacements along isentropic surfaces. As such, a weak meridional tracer gradient along the mixing direction [i.e., $(\partial \bar{q} / \partial \phi)_{(p/p_s)}$ for the QG flow and $(\partial \bar{q} / \partial \phi)_\theta \approx (\partial \bar{q} / \partial \phi)_{(p/p_s)} + (\partial \bar{q} / \partial p)_\theta (\partial p / \partial \phi)_\theta$ for the adiabatic flow] indicates strong eddy mixing and vice versa. In the figure, the weak gradient region (where the tracer gradient is less than 0.1) is highlighted with shading. For both the QG and adiabatic flows, the meridional tracer gradients are weak in the high latitudes or in the lower-level midlatitudes, indicating strong mixing; the tracer gradients are large in the tropics and in the upper-level midlatitudes, indicating weak mixing.

Figure 6 displays snapshots of the horizontal distribution of tracers on day 90 for the QG flow in the left panels and for the adiabatic flow in the right panels. The gray shading highlights the area bounded by the tracer contour with the mass equivalent latitude of 40°N . Consistent with the meridional tracer gradient, the tracer distribution in the upper troposphere (at 225 hPa or 330 K) is wavelike near the jet, and the tracer distribution near the surface (at 775 hPa or 290 K), in contrast, is turbulent with frequent overturning tracer contours. Given the complexity in tracer geometry, a quantitative measure of the flow is needed to understand the effect on tracer transport. It is also important to note that the actual latitude of a tracer contour can be far away from its mass equivalent latitude owing to large displacements of eddies, as exemplified by the mass equivalent latitude of 40°N . The mass equivalent latitude also helps to simplify the treatment of the intersections of isentropes with the ground.

In summary, while the tropical ascent of isopleths and interhemispheric exchange of tracers in the total flow

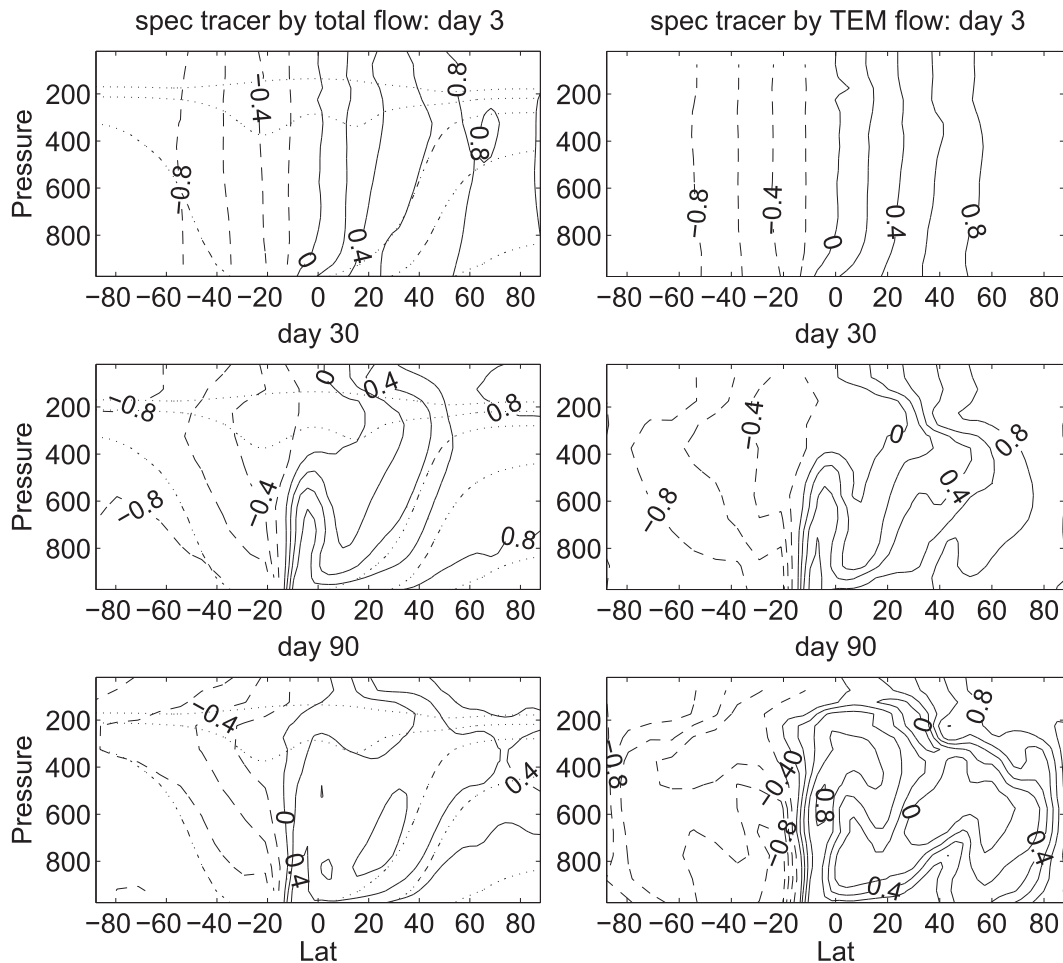


FIG. 4. The zonal mean spectral tracer mixing ratio on (top) day 3, (middle) day 30, and (bottom) day 90, advected by (left) the total flow (expt 1) and (right) the TEM residual circulation (expt 2). The interval of (solid and dashed) contours is 0.2. The dashed-dotted lines in the left panels denote the mean potential temperature, as in Fig. 3. See Table 1 for descriptions of experiments.

are captured only by the simulation advected by the TEM residual circulation, the extratropical tracer isopleth slopes are reproduced only in the simulation advected by the adiabatic flow. The simulation with the QG flow cannot yield either the tropical or extratropical tracer isopleth slopes, but the regions of strong and weak mixing are consistent with those advected by the adiabatic flow. These mixing characteristics are investigated in detail in the following section.

b. Effective eddy diffusivities

Here, we compare the effective eddy diffusivity [Eq. (19)] calculated from the spectral tracers advected by the QG and adiabatic flows. As the primary direction of mixing is different, the effective diffusivity is separately evaluated along the sigma level for the QG flow and along the isentropic surface for the adiabatic flow.

Figure 7 shows the temporal evolution of the QG and isentropic diffusivities averaged during selected days. In the upper troposphere, the QG diffusivity at 225 hPa in the left panels roughly corresponds to the isentropic diffusivity at 330 K in the right panels (cf. Fig. 3), and the two diffusivities agree, at least qualitatively. When averaged over days 100–300, the diffusivity in each hemisphere displays a midlatitude minimum at the jet core ($\sim 45^\circ\text{N}$ or 50°S) with two maxima at the jet's flanks, consistent with the observed pattern of upper-tropospheric diffusivity (Haynes and Shuckburgh 2000b). The diffusivity minimum near 45°N does not emerge during days 1–5, likely influenced by the tracer initial conditions. After day 30, the midlatitude minimum is persistent and the meridional structure of diffusivity remains qualitatively similar, although the values in selected periods differ largely from the 200-day mean. Furthermore, the

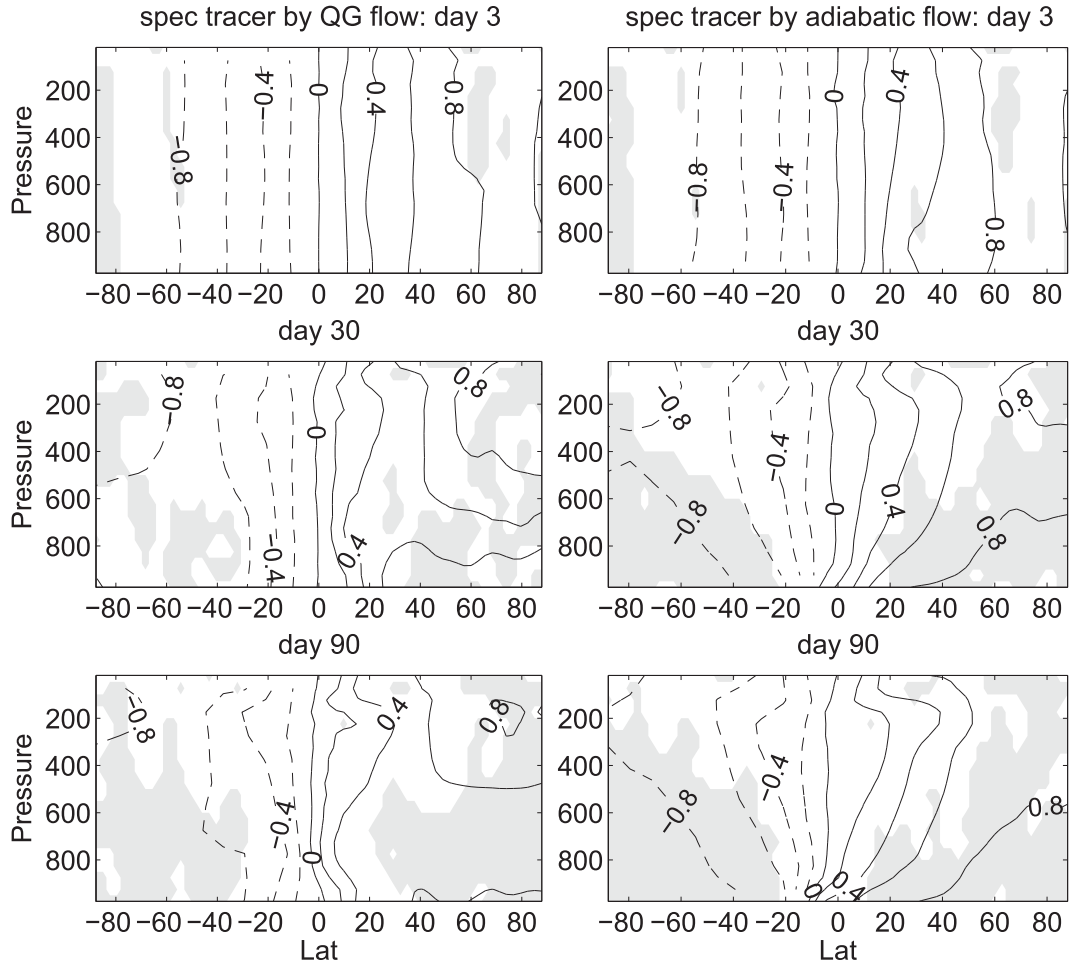


FIG. 5. The zonal mean spectral tracer mixing ratio, as in Fig. 4, but advected by (left) the QG flow (expt 3a) and (right) the adiabatic flow (expt 4a). Contour interval is 0.2. The region of weak meridional tracer gradient is shaded for $(\partial\bar{q}/\partial\phi)_{(p,p_s)} < 0.1$ in the QG flow and for $(\partial\bar{q}/\partial\phi)_\theta < 0.1$ in the adiabatic flow. See Table 1 for descriptions of experiments.

weak midlatitude mixing and strong high-latitude mixing are consistent with the strong midlatitude tracer gradients and weak high-latitude gradients in the upper level on day 90 in Figs. 5 and 6. Note that effective eddy diffusivity is presented at the mass equivalent latitude rather than the actual latitude (see Fig. 6 for their difference).

In the lower troposphere, the QG diffusivity at 775 hPa in the left panels is compared with the isentropic diffusivity at the top of the surface layer (i.e., 95% quantile of surface potential temperature distribution) in the right panels (cf. Fig. 3). The two diffusivities are qualitatively similar. When averaged over days 100–300, both the QG and isentropic diffusivities are large throughout the baroclinic zone with peaks near 45°S and 40°N, consistent with the weak tracer gradients in the lower level on day 90 in Figs. 5 and 6. The isentropic

diffusivity seems to suggest a second maximum in the high latitudes (~70°S/N), and the two diffusivities averaged over selected periods disagree quantitatively especially in the middle and high latitudes. These discrepancies may be attributed to the mixing associated with the vertical parcel displacements along near-surface isentropes (where the isentropic slopes are large) that are ignored in the QG flow.

The vertical structures of the QG and isentropic diffusivities are compared in Fig. 8, and the WMO tropopause and the top of surface layer are denoted by the green lines. In the NH, the QG diffusivity displays a maximum near 700 hPa and 45°N, corresponding to the isentropic diffusivity maximum near 290 K. The diffusivity decreases with altitude from above the top of the surface layer, reaching a minimum at the jet core or at the tropopause. The decrease with altitude is slower at

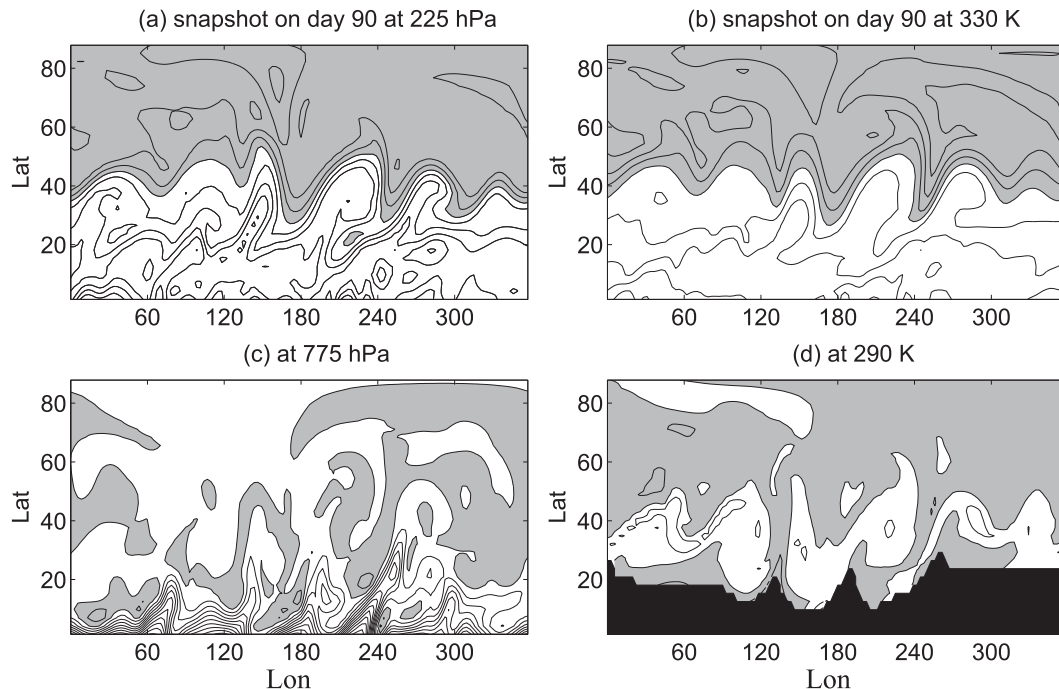


FIG. 6. Snapshot of the horizontal distribution of tracers on day 90. (left) The tracers advected by the QG flow at (a) 225 and (c) 775 hPa (expt 3a). (right) The tracers advected by the adiabatic flow at (b) 330 and (d) 290 K (expt 4a). Contour intervals are 0.1 in (a),(b) and 0.05 in (c),(d). The gray shading indicates the area bounded by the tracer contour that corresponds to the mass equivalent latitude of 40°N . The black shading in (d) indicates the underground.

the jet's flanks. The diffusivity structure in the SH is similar to that in the NH, but the amplitude is weaker. The characteristics of the QG and isentropic diffusivities in this primitive equation model are consistent with those in the QG simulations (Greenslade and Haynes 2008). The diffusivity in the deep tropics is very weak in this dry model owing to the lack of small-scale convection or large-scale stirring, since the equatorward-propagating Rossby waves would break down and get dissipated near their subtropical critical latitudes (e.g., Randel and Held 1991).

Some quantitative differences are also noticeable between the two diffusivities. The low values of effective diffusivity near the midlatitude jet in the QG case are closely tied to the zonal winds (i.e., the diffusivity minimum in blue corresponds to the zonal winds greater than 30 m s^{-1}), whereas in the adiabatic case, the values of effective diffusivity near the midlatitude jet are high below about 310 K, even when the zonal winds are large.

c. Sensitivities to initial tracer distributions

Shuckburgh and Haynes (2003) showed generally for time-periodic flows, the effective diffusivity of a non-divergent advecting flow is independent of initial conditions of tracers except for very weak initial tracer gradients. The effective diffusivities diagnosed with

three different initial tracer distributions are compared in Fig. 9. Indeed, different initial distributions yield nearly identical effective diffusivities for the QG flow and for the adiabatic flow in the upper troposphere. The near-surface isentropic diffusivities show some sensitivities to initial conditions, which may be attributed to strong thermal damping near the surface in the model. As pointed out by Plumb and Ferrari (2005), under strong diabatic heating in the surface layer, the residual eddy tracer transport from removing the TEM circulation may not be exactly along the isentropic surface. In spite of this limitation, the structures of the near-surface isentropic diffusivity with different initial conditions agree qualitatively.

d. Sensitivities to jet strength

The impact of the jet strength on the effective diffusivity is also investigated by altering the parameter for hemispherically asymmetric heating (Fig. 10). For $\epsilon = 0\text{ K}$, the time-mean zonal wind is symmetric about the equator with the jet maximum around 33 m s^{-1} . For $\epsilon = 40\text{ K}$, the zonal wind peaks around 51 m s^{-1} in the NH and around 18 m s^{-1} in the SH. In spite of the large difference in the zonal jet speed between the two simulations, we see a robust midlatitude diffusivity minimum at the jet core for both the QG flow and adiabatic

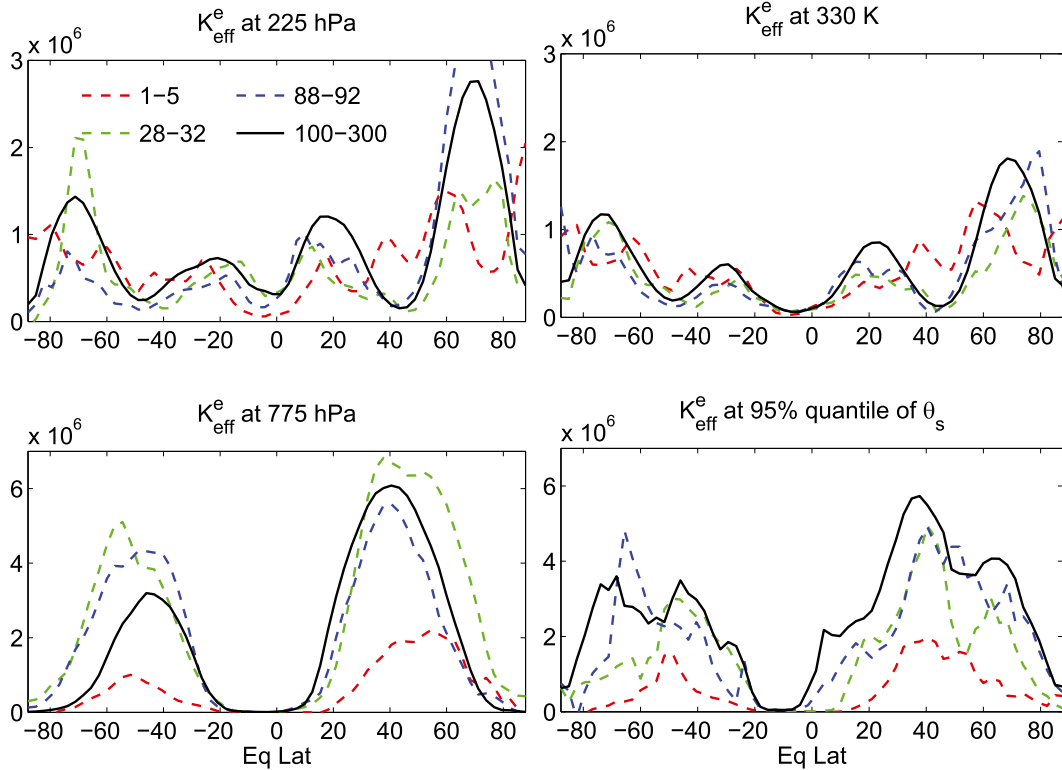


FIG. 7. Effective eddy diffusivity ($\text{m}^2 \text{s}^{-1}$) averaged for days 1–5, 28–32, 88–92, and 100–300. (left) Values are calculated from the tracers advected by the QG flow at (top) 225 and (bottom) 775 hPa (expt 3a). (right) Values are calculated from the tracers advected by the adiabatic flow at (top) 330 K and (bottom) 95% quantile of surface potential temperature distribution (expt 4a). The effective diffusivity is calculated from spectral tracers with Eq. (19).

flow, surrounded by larger values in diffusivity at the jet’s two flanks. Interestingly, for the case of $\epsilon = 40 \text{ K}$, the diffusivity maximum on the equatorward flank of the wintertime subtropical jet encroaches into the regions of

tropical easterlies, indicating a vigorous nonlinear critical layer. In the lower troposphere (below 500 hPa or 310 K), the diffusivity is characterized by a midlatitude maximum below the jet and the diffusivity spreads

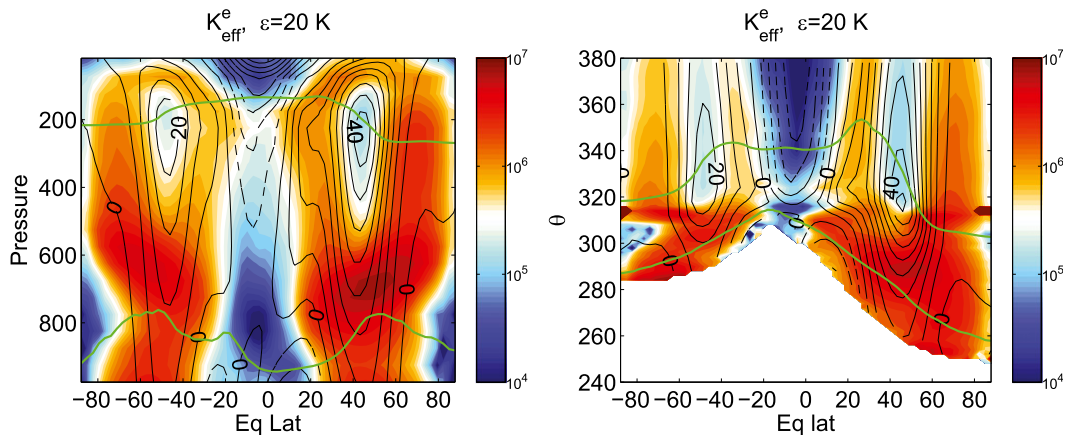


FIG. 8. Effective eddy diffusivity (shading; $\text{m}^2 \text{s}^{-1}$) and zonal wind (black contours; m s^{-1}) averaged for days 100–300. Values are calculated from the tracers advected by (left) the QG flow (expt 3a) and (right) the adiabatic flow (expt 4a). The effective diffusivity is calculated from spectral tracers by Eq. (19). Contour intervals for the zonal winds are 5 m s^{-1} . The green lines indicate the WMO tropopause and the 95% quantile of surface potential temperature distribution θ_s . The diffusivity for the isentropes less than the 10% quantile of θ_s is not shown.

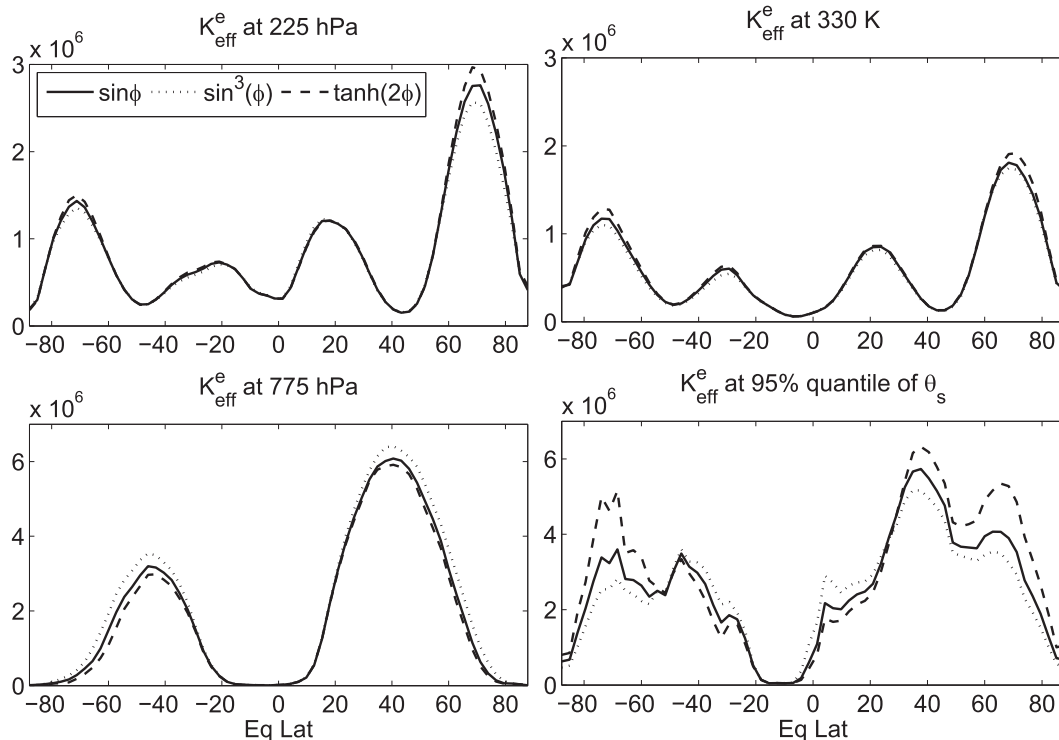


FIG. 9. Effective diffusivity ($\text{m}^2 \text{s}^{-1}$) averaged for days 100–300, as in Fig. 7, but for three initial tracer distributions: $\sin(\phi)$, $\sin^3(\phi)$, and $\tanh(2\phi)$. (left) Values are calculated from spectral tracers advected by the QG flow at (top) 225 and (bottom) 775 hPa (expts 3a–3c), and (right) values are calculated from the tracers advected by the adiabatic flow at (top) 330 K and (bottom) 95% quantile of surface potential temperature (expts 4a–4c).

throughout the baroclinic zone. When ϵ is not zero, the effective diffusivity is larger in the winter hemisphere than the summer hemisphere, consistent with the observed seasonal difference in eddy diffusivity inferred from the energy transport (e.g., Stone and Miller 1980).

The diffusivity maxima at the jet's flanks and the minimum at the jet core are compared with the zonal jet speed in Fig. 11 for ϵ varied from 0 to 40 K with an interval of 10 K. The contrast between the midlatitude minimum and subtropical and/or subpolar values is larger for the jet with a larger zonal speed, as expected from larger baroclinicity and more energetic baroclinic eddies that break down on the jet's flanks. Also, a stronger zonal jet can suppress the mixing at the jet core by acting as a more effective mixing barrier [see also Haynes and Shuckburgh (2000b)].

While our results agree qualitatively with the observed seasonal cycle of effective diffusivity in Haynes and Shuckburgh (2000b), some quantitative differences in the region of weak mixing can be attributed to the differences in the diagnostic method. Haynes and Shuckburgh (2000b) use the regular diffusion with $\kappa = 3.24 \times 10^5 \text{m}^2 \text{s}^{-1}$, and this sets a minimum effective diffusivity in the absence of eddy stirring. As shown in Figs. 8 and 10, the effective eddy diffusivity in our

diagnostic can be much smaller than this minimum, and it would be zero without stirring [see Eq. (22)]. Also, when the hyperdiffusion is used rather than the regular diffusion, the effective diffusivity is not restricted by such a diffusivity minimum [see also Nakamura and Zhu (2010)]. Despite these differences, the time-mean effective eddy diffusivity is positive, indicating down-gradient eddy tracer fluxes.

e. Sensitivities to numerical schemes of small-scale diffusion

The spectral diffusion is often not desirable for tracer transport because of the nonlocal Gibbs effect. For all the tracer transport experiments, we have repeated the transport calculation with a grid tracer advected by a semi-Lagrangian scheme for horizontal advection, and the grid tracer generally agrees with the spectral tracer advected by the same circulation. To show this, we calculate eddy mixing by the equivalent length [Eq. (23)] for the spectral and grid tracers advected by the same adiabatic flow for $\epsilon = 20 \text{K}$. Despite different numerical schemes, Fig. 12 shows a very good agreement in eddy mixing in terms of the tracer equivalent length, with consistent eddy diffusivity maxima and minima between the two schemes. A careful analysis of the diffusivity

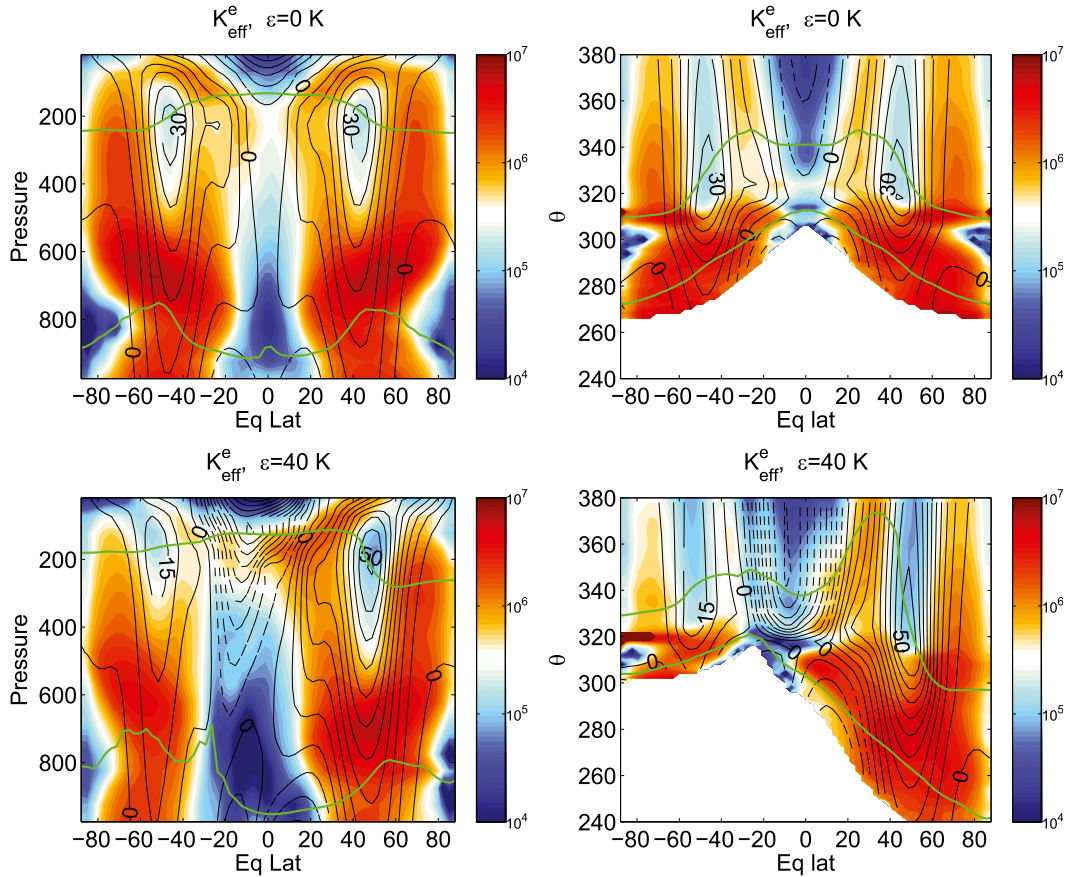


FIG. 10. Effective eddy diffusivity (shading; $\text{m}^2 \text{s}^{-1}$) and zonal winds (black contours; m s^{-1}), as in Fig. 8, but for (top) $\epsilon = 0$ and (bottom) $\epsilon = 40 \text{ K}$. (left) Values are calculated from spectral tracers advected by (left) the QG flow (expts 5a and 5d), and (right) the adiabatic flow (expts 6a and 6d). Contour intervals for the zonal winds are 5 m s^{-1} . The green lines indicate the WMO tropopause and the 95% quantile of θ_s .

magnitude for the 330-K isentrope and the near-surface flow indicates that the equivalent length of the spectral tracer is larger than that of the grid tracer (Fig. 13). As the equivalent length quantifies the complexity in tracer geometry, this is consistent with the snapshot of tracer contours that the spectral tracer has slightly more fine-scale chaotic structures than the grid tracer (not shown). This suggests that the ∇^8 hyperdiffusion is slightly less diffusive than the semi-Lagrangian scheme.

Using a global tracer variance budget described in Allen and Nakamura (2001), we can parameterize the decay of the global-mean tracer variance by a regular diffusion, and the diffusion coefficient is estimated as $\kappa \approx 1 \times 10^5 \text{ m}^2 \text{ s}^{-1}$ for both spectral and grid tracers. This leads to an approximate effective isentropic diffusivity as $K_{\text{eff}}^e = \tilde{K}_{\text{eff}}^e \times 10^5 \text{ m}^2 \text{ s}^{-1}$. While the isentropic diffusivity derived with this approach differs quantitatively from the diffusivity calculated directly with the small-scale diffusion (cf. the right panels of Figs. 9 and 13), the spatial pattern in Fig. 12 is generally comparable with the direct

estimate in Fig. 8. The similarity between the equivalent length ratios of the spectral and grid tracers supports previous studies that the effective diffusivity of the troposphere and stratosphere, where eddy mixing is dominated by large-scale stirring, is largely dictated by large-scale stirring rather than the small-scale diffusion scheme used (e.g., Allen and Nakamura 2001; Shuckburgh and Haynes 2003; Marshall et al. 2006; Leibensperger and Plumb 2014).

Shuckburgh and Haynes (2003) and Marshall et al. (2006) found that the effective diffusivity of tracer transport becomes independent of the small-scale diffusion in the circulation regime where the Peclet number (approximately the square of the ratio of eddy length scale and Batchelor scale) exceeds 50. In this circulation regime, the Peclet number scales with the equivalent length ratio of tracer contours, which should also be greater than 50. Figure 13 suggests the current model resolution is not sufficient for this circulation regime. Also, Eq. (22) indicates a weak sensitivity of eddy

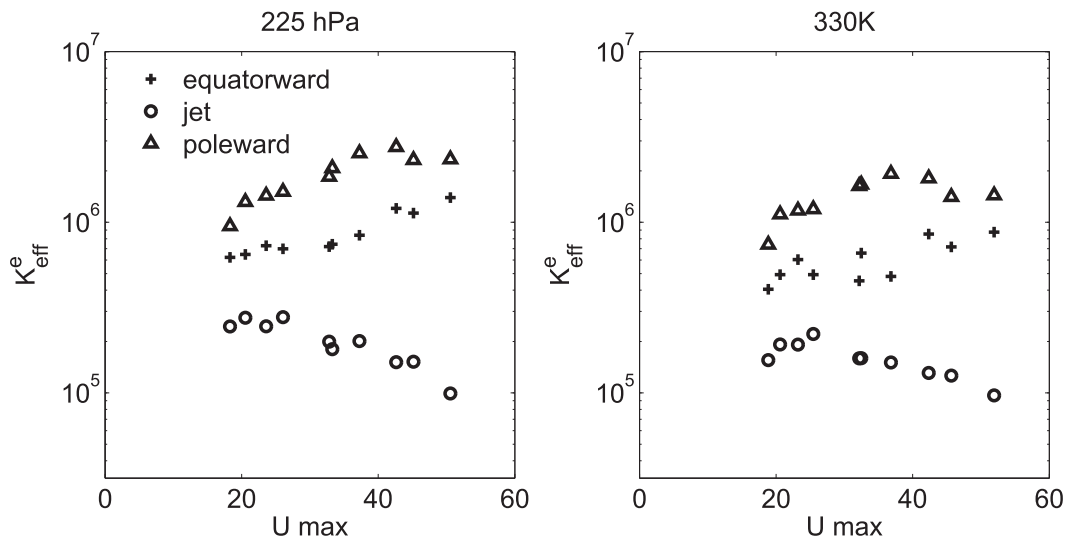


FIG. 11. Effective eddy diffusivities at the jet's flanks and at the jet core vs the zonal jet speed maximum at (left) 225 hPa and (right) 330 K. The results are for the experiments in which ε is 0, 10, 20, 30, and 40 K. Both hemispheres are included, with larger zonal jet speeds for the winter hemisphere. Plus signs and triangles indicate the effective diffusivity maxima on the jet's equatorward and poleward flanks, respectively, and circles indicate the diffusivity minimum at the jet core [see the top panels of Fig. 9 for examples]. Values are calculated from spectral tracers advected by (left) the QG flow (expts 3a and 5a–5d) and from tracers advected by (right) the adiabatic flow (expts 4a and 6a–6d).

diffusivity to the diffusion coefficient even when the effective diffusivity becomes independent of the coefficient. Therefore, the exact magnitude of effective eddy diffusivity diagnosed in our study is likely sensitive to the resolution of the model examined, although the pattern is expected to remain unchanged.

5. Conclusions and discussion

A theoretical framework for the effective isentropic diffusivity of tropospheric transport is presented. Compared with previous isentropic analysis (Haynes and

Shuckburgh 2000a,b; Allen and Nakamura 2001), we develop a diffusivity diagnostic that allows the isentropes to intersect with the ground frequently. Using the small-scale diffusion experienced by the tracer, the effective diffusivity can account for both the horizontal and vertical parcel displacements in the near-surface isentropic flow. Furthermore, this effective diffusivity is directly linked to a diffusive closure of eddy fluxes through a finite-amplitude wave activity equation.

The role of atmospheric circulation in the tracer transport is investigated in the idealized simulations of a primitive equation model, and the effects of the advecting

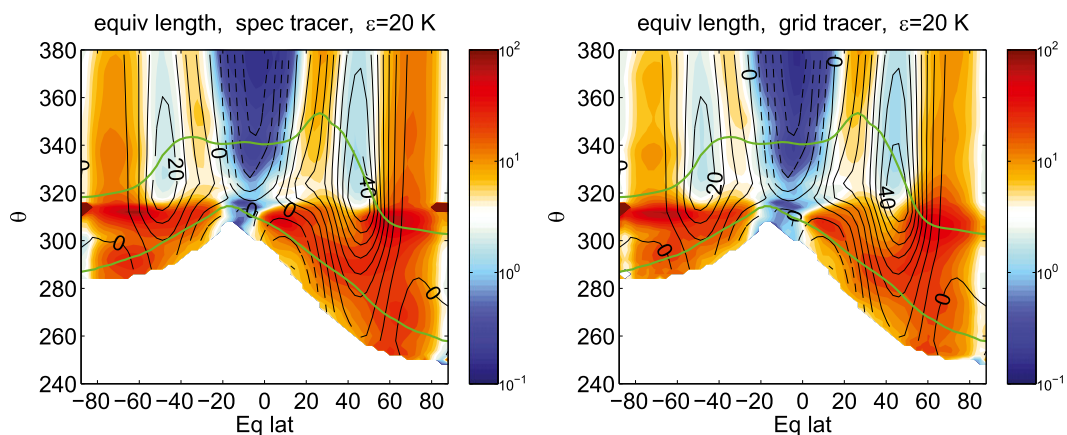


FIG. 12. Eddy equivalent length ratio (shading) and zonal wind (black contours) averaged for days 100–300, as in Fig. 8. The eddy equivalent length ratio is calculated by Eq. (23) from (left) spectral tracer (expt 4a) and (right) grid tracer (expt 7) advected by the same adiabatic flow. Contour intervals for the zonal winds are 5 m s^{-1} .

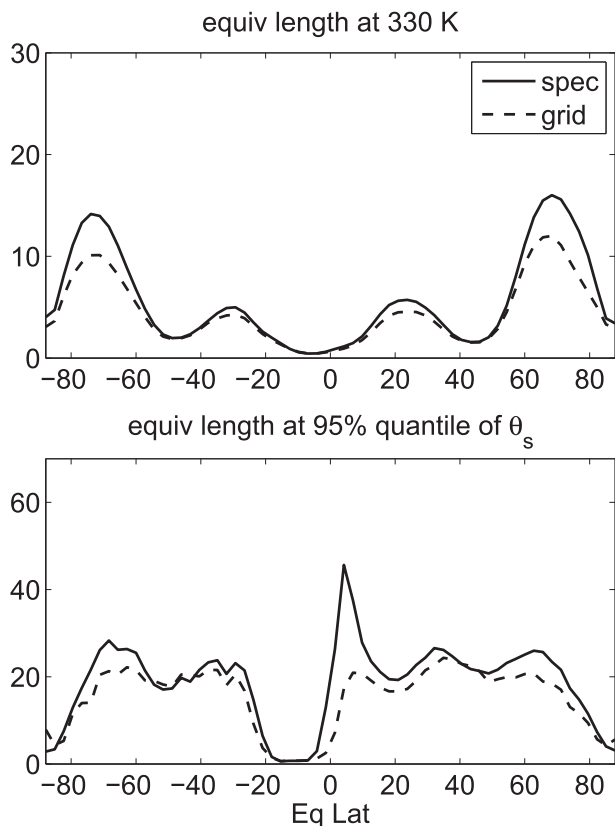


FIG. 13. Eddy equivalent length ratio averaged for days 100–300, as in Fig. 12, but for (top) 330 K and (bottom) 95% quantile of surface potential temperature. Solid (dashed) lines denote the spectral (grid) tracer.

flow are separated with different components of the flow [i.e., total, TEM, quasigeostrophic (QG), and adiabatic flows]. While the tropical ascent of tracer isopleths and interhemispheric exchange of tracers in the total flow are captured by the simulation advected by the TEM residual circulation, the extratropical tracer isopleth slopes are reproduced only in the simulation advected by the adiabatic flow. The simulation with the QG flow cannot yield either the tropical or extratropical tracer isopleth slopes, but the regions of strong and weak mixing agree with those advected by the adiabatic flow. These individual roles of diabatic circulation and eddy mixing in tropospheric transport are consistent with our understandings of their roles in stratospheric transport (e.g., Holton 1986; Mahlman et al. 1986).

The effective diffusivity is evaluated for the QG flow along the model level and for the adiabatic flow along the isentropic surface, respectively. Although the directions of eddy mixing and the resulting tracer isopleth slopes are different for the QG flow and adiabatic flow, the patterns of effective diffusivities agree well: the upper troposphere is characterized by a diffusivity minimum at

the jet’s center with enhanced mixing at the jet’s flanks, and the lower troposphere is dominated by stronger mixing throughout the baroclinic zone. These diffusivity patterns are relatively independent of the initial tracer gradients and are qualitatively similar with altered jet speeds. Furthermore, the isentropic diffusivity agrees broadly with the equivalent lengths of tracer contours by using either a spectral diffusion scheme or a semi-Lagrangian advection scheme. These results provide additional evidence to tropospheric mixing characteristics (Fig. 1) in previous studies with the single isentropic layer model (e.g., Haynes and Shuckburgh 2000b; Allen and Nakamura 2001) or the QG model (e.g., Greenslade and Haynes 2008).

These results above also indicate that our understandings of eddy mixing in the troposphere from the QG theory can be applied, at least qualitatively, to the isentropic flow that intersects the ground. However, this does not mean that the vertical parcel displacement is unimportant. We have mainly considered quasi-horizontal diffusion in our numerical calculation, but in reality the vertical diffusion associated with the vertical parcel displacement can be important (Haynes and Anglade 1997). Leibensperger and Plumb (2014) considered both horizontal and vertical diffusions and found that the resulting effective diffusivities for horizontal and vertical diffusions are qualitatively similar.

It should be noted that the idealized dry model examined has not included the effects of small-scale convection and associated vertical diffusion on tracer transport. It is expected that convection can generate stirring (e.g., Rossby waves) in addition to the baroclinic instability in the dry model. However, the resemblance of our results to the seasonal cycle of effective diffusivity in observations (e.g., Haynes and Shuckburgh 2000b) indicates that our results can hold qualitatively even in the presence of moisture. This is consistent with the results that global-scale tracer transport in the model simulations with and without convective transport are qualitatively similar (Erukhimova and Bowman 2006; Hess 2005).

While previous works on effective diffusivity focus on long-lived tracers, the wave activity budget in Eq. (29) can be readily extended to include nonnegligible sources or sinks of tracers other than the small-scale diffusion. This can be particularly useful to understand the up-gradient PV fluxes near the subtropical jet. While our idealized model can simulate the up-gradient eddy PV flux near the jet (Fig. 3d), the time-mean effective diffusivity of the adiabatic flow is positive (Fig. 8), implying that the adiabatic eddy tracer fluxes are downgradient. This indicates that diabatic heating may be important for these up-gradient fluxes, although a complete wave activity budget of the isentropic PV is needed to resolve

this issue. Similarly, one may analyze the wave activity budget of air pollutants to understand the effect of diabatic heating, isentropic mixing, emission, and deposition on their global-scale transport.

The gradient–flux relationships for quasi-conservative tracers have been derived for small-amplitude waves (Plumb 1979; Matsuno 1980; Holton 1981) and for finite-amplitude eddies in the QG flow (Nakamura and Zhu 2010). Our theoretical framework has extended these works to pure horizontal flow in a general vertical coordinate. An improved understanding of the eddy diffusivity is valuable for many aspects of the global atmospheric circulation such as atmospheric energy transport (e.g., Held and Larichev 1996; Lapeyre and Held 2003), the height of extratropical tropopause (e.g., Haynes and Shuckburgh 2000a; Jansen and Ferrari 2013), or the latitude of surface westerly winds (e.g., Chen et al. 2013).

Acknowledgments. We thank Eric Leibensperger, Noboru Nakamura, Peter Hess, and Lantao Sun for valuable discussion. We are also grateful for three anonymous reviewers for constructive comments. GC is supported by the National Science Foundation (NSF) Climate and Large-Scale Dynamics program under Grants AGS-1042787 and AGS-1064079.

APPENDIX

Small-Amplitude Limit of Effective Eddy Diffusivity [Eq. (26)]

Consider a small-amplitude perturbation with the tracer contour Q disturbed from the latitude ϕ_e by a small displacement $\delta\phi_e(\lambda) = \phi(\lambda, Q) - \phi_e$, where $\phi(\lambda, Q)$ is the latitude of the tracer contour, and we allow possible intersections with the ground but with no reversal of the tracer gradient for a small-amplitude wave. For a conservative disturbance, the eddy component of q can be approximated as

$$\hat{q} \equiv q - \bar{q}^* \approx -\delta\phi_e \frac{\partial Q}{\partial \phi_e}. \quad (\text{A1})$$

From the definition of the mass equivalent latitude [Eq. (7)] that deals with the ground intersections, we have

$$\overline{\sigma \delta\phi_e} \approx \frac{1}{\cos(\phi_e)} \int_{\phi_e}^{\phi_e + \delta\phi_e(\lambda)} \sigma \cos(\phi) d\phi = 0. \quad (\text{A2})$$

Using the displacement, the operator $\Delta\mathcal{M}(\hat{q})$ in Eq. (20) can be written as

$$\Delta\mathcal{M}(\hat{q}) = -\frac{a}{\cos(\phi_e)} \int_{\phi_e}^{\phi_e + \delta\phi_e(\lambda)} \sigma \hat{q} \cos(\phi) d\phi. \quad (\text{A3})$$

Substituting with $\hat{q} \equiv \bar{q}^* + \hat{q}$ and Eq. (A2), we have

$$\begin{aligned} \Delta\mathcal{M}(\hat{q}) &\approx -\frac{a}{\cos(\phi_e)} \left[\int_{\phi_e}^{\phi_e + \delta\phi_e(\lambda)} \sigma \hat{q} \cos(\phi) d\phi \right. \\ &\quad \left. + \bar{q}^* \int_{\phi_e}^{\phi_e + \delta\phi_e(\lambda)} \sigma \cos(\phi) d\phi \right] \\ &\approx -a \overline{\sigma (\hat{q} \delta\phi_e)}^* = a \overline{\sigma} \frac{\overline{\hat{q} \hat{q}}^*}{\partial Q / \partial \phi_e}, \end{aligned} \quad (\text{A4})$$

where we have substituted with Eq. (A1) in the final equality. Therefore, the small-amplitude approximation of the effective diffusivity [Eq. (19)] can be written as

$$K_{\text{eff}}^e = -\frac{a}{\overline{\sigma}} \left(\frac{\partial Q}{\partial \phi_e} \right)^{-1} \Delta\mathcal{M}(\hat{q}) = -a^2 \left(\frac{\partial Q}{\partial \phi_e} \right)^{-2} \overline{\hat{q} \hat{q}}^*. \quad (\text{A5})$$

For pure horizontal diffusion $\hat{q} = (1/\sigma) \nabla_\eta \cdot (\sigma \kappa_h \nabla_\eta q)$, we have

$$\begin{aligned} \overline{\hat{q} \hat{q}}^* &= \frac{1}{\overline{\sigma}} \overline{[\hat{q} \nabla_\eta \cdot (\sigma \kappa_h \nabla_\eta \hat{q})]} \\ &= \frac{1}{\overline{\sigma}} \left\{ \overline{\nabla_\eta \cdot \left[\sigma \kappa_h \nabla_\eta \left(\frac{\hat{q}^2}{2} \right) \right]} - \overline{\sigma \kappa_h |\nabla_\eta \hat{q}|^2} \right\} \\ &\approx -\overline{\kappa_h |\nabla_\eta \hat{q}|^2}^*, \end{aligned} \quad (\text{A6})$$

where we have assumed that the horizontal diffusion of \hat{q}^2 is small.

Similarly, for pure vertical diffusion $\hat{q} = (1/\sigma) (\partial/\partial \eta) [\sigma \kappa_v (\partial \eta / \partial z)^2 (\partial q / \partial \eta)]$, we have

$$\begin{aligned} \overline{\hat{q} \hat{q}}^* &= \frac{1}{\overline{\sigma}} \left\{ \overline{\hat{q} \frac{\partial}{\partial \eta} \left[\sigma \kappa_v \left(\frac{\partial \eta}{\partial z} \right)^2 \frac{\partial \hat{q}}{\partial \eta} \right]} \right\} \\ &= \frac{1}{\overline{\sigma}} \left\{ \overline{\frac{\partial}{\partial \eta} \left[\sigma \kappa_v \left(\frac{\partial \eta}{\partial z} \right)^2 \frac{\partial}{\partial \eta} \left(\frac{\hat{q}^2}{2} \right) \right]} \right. \\ &\quad \left. - \overline{\sigma \kappa_v \left(\frac{\partial \eta}{\partial z} \right)^2 \left(\frac{\partial \hat{q}}{\partial \eta} \right)^2} \right\} \\ &\approx -\overline{\kappa_v \left(\frac{\partial \eta}{\partial z} \right)^2 \left(\frac{\partial \hat{q}}{\partial \eta} \right)^2}^*, \end{aligned} \quad (\text{A7})$$

where we have that assumed the vertical diffusion of \hat{q}^2 is small.

Substituting Eqs. (A6) and (A7) into Eq. (A5) yields Eq. (26).

REFERENCES

- Allen, D. R., and N. Nakamura, 2001: A seasonal climatology of effective diffusivity in the stratosphere. *J. Geophys. Res.*, **106**, 7917–7935, doi:10.1029/2000JD900717.
- Andrews, D. G., and M. E. McIntyre, 1978: Generalized Eliassen–Palm and Charney–Drazin theorems for waves on axisymmetric mean flows in compressible atmospheres. *J. Atmos. Sci.*, **35**, 175–185.
- , J. R. Holton, and C. B. Leovy, 1987: *Middle Atmosphere Dynamics*. International Geophysics Series, Vol. 40, Academic Press, 489 pp.
- Birner, T., D. W. J. Thompson, and T. G. Shepherd, 2013: Up-gradient eddy fluxes of potential vorticity near the subtropical jet. *Geophys. Res. Lett.*, **40**, 5988–5993, doi:10.1002/2013GL057728.
- Bowman, K. P., and G. D. Carrie, 2002: The mean-meridional transport circulation of the troposphere in an idealized GCM. *J. Atmos. Sci.*, **59**, 1502–1514, doi:10.1175/1520-0469(2002)059<1502:TMMTCO>2.0.CO;2.
- , and T. Erukhimova, 2004: Comparison of global-scale Lagrangian transport properties of the NCEP reanalysis and CCM3. *J. Climate*, **17**, 1135–1146, doi:10.1175/1520-0442(2004)017<1135:COGLTP>2.0.CO;2.
- Butchart, N., and E. E. Remsberg, 1986: The area of the stratospheric polar vortex as a diagnostic for tracer transport on an isentropic surface. *J. Atmos. Sci.*, **43**, 1319–1339, doi:10.1175/1520-0469(1986)043<1319:TAOTSP>2.0.CO;2.
- Chen, G., 2013: The mean meridional circulation of the atmosphere using the mass above isentropes as the vertical coordinate. *J. Atmos. Sci.*, **70**, 2197–2213, doi:10.1175/JAS-D-12-0239.1.
- , J. Lu, and L. Sun, 2013: Delineating the eddy–zonal flow interaction in the atmospheric circulation response to climate forcing: Uniform SST warming in an idealized aquaplanet model. *J. Atmos. Sci.*, **70**, 2214–2233, doi:10.1175/JAS-D-12-0248.1.
- Erukhimova, T., and K. P. Bowman, 2006: Role of convection in global-scale transport in the troposphere. *J. Geophys. Res.*, **111**, D03105, doi:10.1029/2005JD006006.
- Greenslade, M. D., and P. H. Haynes, 2008: Vertical transition in transport and mixing in baroclinic flows. *J. Atmos. Sci.*, **65**, 1137–1157, doi:10.1175/2007JAS2236.1.
- Haynes, P. H., and J. Anglade, 1997: The vertical-scale cascade in atmospheric tracers due to large-scale differential advection. *J. Atmos. Sci.*, **54**, 1121–1136, doi:10.1175/1520-0469(1997)054<1121:TVSCIA>2.0.CO;2.
- , and E. F. Shuckburgh, 2000a: Effective diffusivity as a diagnostic of atmospheric transport: 1. Stratosphere. *J. Geophys. Res.*, **105**, 22 777–22 794, doi:10.1029/2000JD900093.
- , and —, 2000b: Effective diffusivity as a diagnostic of atmospheric transport: 2. Troposphere and lower stratosphere. *J. Geophys. Res.*, **105**, 22 795–22 810, doi:10.1029/2000JD900092.
- Held, I. M., and M. J. Suarez, 1994: A proposal for the intercomparison of the dynamical cores of atmospheric general circulation models. *Bull. Amer. Meteor. Soc.*, **75**, 1825–1830, doi:10.1175/1520-0477(1994)075<1825:APFTIO>2.0.CO;2.
- , and V. D. Larichev, 1996: A scaling theory for horizontally homogeneous, baroclinically unstable flow on a beta plane. *J. Atmos. Sci.*, **53**, 946–952, doi:10.1175/1520-0469(1996)053<0946:ASTFHH>2.0.CO;2.
- Hess, P. G., 2005: A comparison of two paradigms: The relative global roles of moist convective versus nonconvective transport. *J. Geophys. Res.*, **110**, D20302, doi:10.1029/2004JD005456.
- Holton, J. R., 1981: An advective model for two-dimensional transport of stratospheric trace species. *J. Geophys. Res.*, **86**, 11 989–11 994, doi:10.1029/JC086iC12p11989.
- , 1986: A dynamically based transport parameterization for one-dimensional photochemical models of the stratosphere. *J. Geophys. Res.*, **91**, 2681–2686, doi:10.1029/JD091iD02p02681.
- Jansen, M., and R. Ferrari, 2013: The vertical structure of the eddy diffusivity and the equilibration of the extratropical atmosphere. *J. Atmos. Sci.*, **70**, 1456–1469, doi:10.1175/JAS-D-12-086.1.
- Lapeyre, G., and I. M. Held, 2003: Diffusivity, kinetic energy dissipation, and closure theories for the poleward eddy heat flux. *J. Atmos. Sci.*, **60**, 2907–2916, doi:10.1175/1520-0469(2003)060<2907:DKEDAC>2.0.CO;2.
- Lee, S., and I. M. Held, 1993: Baroclinic wave packets in models and observations. *J. Atmos. Sci.*, **50**, 1413–1428, doi:10.1175/1520-0469(1993)050<1413:BWPIMA>2.0.CO;2.
- Leibensperger, E. M., and R. A. Plumb, 2014: Effective diffusivity in baroclinic flow. *J. Atmos. Sci.*, **71**, 972–984, doi:10.1175/JAS-D-13-0217.1.
- Lin, S.-J., W. C. Chao, Y. C. Sud, and G. K. Walker, 1994: A class of the van Leer-type transport schemes and its application to the moisture transport in a general circulation model. *Mon. Wea. Rev.*, **122**, 1575–1593, doi:10.1175/1520-0493(1994)122<1575:ACOTVL>2.0.CO;2.
- Mahlman, J. D., H. Levy II, and W. J. Moxim, 1986: Three-dimensional simulations of stratospheric N₂O: Predictions for other trace constituents. *J. Geophys. Res.*, **91**, 2687–2707, doi:10.1029/JD091iD02p02687.
- Marshall, J., E. F. Shuckburgh, H. Jones, and C. Hill, 2006: Estimates and implications of surface eddy diffusivity in the Southern Ocean derived from tracer transport. *J. Phys. Oceanogr.*, **36**, 1806–1821, doi:10.1175/JPO2949.1.
- Matsuno, T., 1980: Lagrangian motion of air parcels in the stratosphere in the presence of planetary waves. *Pure Appl. Geophys. (PAGEOPH)*, **118**, 189–216, doi:10.1007/BF01586451.
- Nakamura, N., 1995: Modified Lagrangian-mean diagnostics of the stratospheric polar vortices. Part I. Formulation and analysis of GFDL SKYHI GCM. *J. Atmos. Sci.*, **52**, 2096–2108, doi:10.1175/1520-0469(1995)052<2096:MLMDOT>2.0.CO;2.
- , 1996: Two-dimensional mixing, edge formation, and permeability diagnosed in an area coordinate. *J. Atmos. Sci.*, **53**, 1524–1537, doi:10.1175/1520-0469(1996)053<1524:TDMEFA>2.0.CO;2.
- , 1998: Leaky containment vessels of air: A Lagrangian-mean approach to the stratospheric tracer transport. *Dynamics of Atmospheric Flows: Atmospheric Transport and Diffusion Processes*, M. P. Singh and S. Raman, Eds., WIT Press, 193–246.
- , and D. Zhu, 2010: Finite-amplitude wave activity and diffusive flux of potential vorticity in eddy–mean flow interaction. *J. Atmos. Sci.*, **67**, 2701–2716, doi:10.1175/2010JAS3432.1.
- , and A. Solomon, 2011: Finite-amplitude wave activity and mean flow adjustments in the atmospheric general circulation. Part II: Analysis in the isentropic coordinate. *J. Atmos. Sci.*, **68**, 2783–2799, doi:10.1175/2011JAS3685.1.
- Plumb, R. A., 1979: Eddy fluxes of conserved quantities by small-amplitude waves. *J. Atmos. Sci.*, **36**, 1699–1704, doi:10.1175/1520-0469(1979)036<1699:EFQCQB>2.0.CO;2.
- , and J. D. Mahlman, 1987: The zonally averaged transport characteristics of the GFDL general circulation/transport model.

- J. Atmos. Sci.*, **44**, 298–327, doi:[10.1175/1520-0469\(1987\)044<0298:TZATCO>2.0.CO;2](https://doi.org/10.1175/1520-0469(1987)044<0298:TZATCO>2.0.CO;2).
- , and R. Ferrari, 2005: Transformed Eulerian-mean theory. Part I: Nonquasigeostrophic theory for eddies on a zonal-mean flow. *J. Phys. Oceanogr.*, **35**, 165–174, doi:[10.1175/JPO-2669.1](https://doi.org/10.1175/JPO-2669.1).
- Randel, W. J., and I. M. Held, 1991: Phase speed spectra of transient eddy fluxes and critical layer absorption. *J. Atmos. Sci.*, **48**, 688–697, doi:[10.1175/1520-0469\(1991\)048<0688:PSSOTE>2.0.CO;2](https://doi.org/10.1175/1520-0469(1991)048<0688:PSSOTE>2.0.CO;2).
- Shuckburgh, E. F., and P. H. Haynes, 2003: Diagnosing transport and mixing using a tracer-based coordinate system. *Phys. Fluids*, **15**, 3342, doi:[10.1063/1.1610471](https://doi.org/10.1063/1.1610471).
- Stone, P. H., and D. Miller, 1980: Empirical relations between seasonal changes in meridional temperature gradients and meridional fluxes of heat. *J. Atmos. Sci.*, **37**, 1708–1721, doi:[10.1175/1520-0469\(1980\)037<1708:ERBSCI>2.0.CO;2](https://doi.org/10.1175/1520-0469(1980)037<1708:ERBSCI>2.0.CO;2).
- Tanaka, D., T. Iwasaki, S. Uno, M. Ujiie, and K. Miyazaki, 2004: Eliassen–Palm flux diagnosis based on isentropic representation. *J. Atmos. Sci.*, **61**, 2370–2383, doi:[10.1175/1520-0469\(2004\)061<2370:EFDBOI>2.0.CO;2](https://doi.org/10.1175/1520-0469(2004)061<2370:EFDBOI>2.0.CO;2).
- Tung, K. K., 1986: Nongeostrophic theory of zonally averaged circulation. Part I: Formulation. *J. Atmos. Sci.*, **43**, 2600–2618, doi:[10.1175/1520-0469\(1986\)043<2600:NTOZAC>2.0.CO;2](https://doi.org/10.1175/1520-0469(1986)043<2600:NTOZAC>2.0.CO;2).